SIMULATION OF A CONFIGURABLE HYBRID AIRCRAFT

A Thesis

presented to

the Faculty of California Polytechnic State University,

San Luis Obispo

In Partial Fulfillment

of the Requirements for the Degree

Master of Science in Aerospace Engineering

by

Brandon Kyle Bartlett

June 2021

COMMITTEE MEMBERSHIP

TITLE:	Simulation of a Configurable Hybrid Aircraft
AUTHOR:	Brandon Kyle Bartlett
DATE SUBMITTED:	June 2021
COMMITTEE CHAIR:	Paulo Iscold, Ph.D. Associate Professor of Aerospace Engineering
COMMITTEE MEMBER:	Aaron Drake, Ph.D. Professor of Aerospace Engineering
COMMITTEE MEMBER:	Dianne DeTurris, Ph.D. Professor of Aerospace Engineering
COMMITTEE MEMBER:	Leonardo Torres, Ph.D. Associate Professor of Aerospace Engineering
COMMITTEE MEMBER:	Kendrick Dlima Systems Engineer, Boeing

ABSTRACT

Simulation of a Configurable Hybrid Aircraft

Brandon Kyle Bartlett

As the demand for air transportation is projected to increase, the environmental impacts produced by air travel will also increase. In order to counter the environmental impacts while also meeting the demand for air travel, there are goals and research initiatives that aim to develop more efficient aircraft. An emerging technology that supports these goals is the application of hybrid propulsion to aircraft, but there is a challenge in effectively exploring the performance of hybrid aircraft due to the time and money required for safe flight testing and due to the diverse design space of hybrid architectures and components. Therefore, computational tools that are capable of simulating the performance of a hybrid aircraft are incredibly useful in the design process and research space.

Existing work on the simulation of hybrid aircraft focuses on modelling a specific hybrid propulsion system in a particular airframe, but it would be desirable to have a simulation tool that is not specific to one design. In this thesis, a simulation framework that can be easily configured for different types of hybrid structures and components is presented, and the simulator is validated using flight test data which demonstrates that the performance of the simulated aircraft is representative of a real aircraft. A design for a hybrid aircraft is also modelled and simulated over different flight profiles in order to study the performance of the hybrid propulsion system. Results indicate that the hybrid aircraft can be successfully simulated and demonstrate how the simulator can be used as a tool to study the best way to fly and operate a hybrid aircraft.

ACKNOWLEDGMENTS

Thanks to:

- My parents and family, for their continuous support throughout my education, especially as a student at Cal Poly.
- My thesis advisor, Dr. Iscold, for inspiring my interest in aircraft performance and taking me on as a graduate student. I am greatly appreciative for all of the informative feedback and guidance that set me on a course for success.
- All of my professors, for making my undergraduate and graduate education a formative experience.
- My friends and roommates, for all the good memories inside and outside of the classroom.
- My girlfriend, for being so supportive throughout the thesis and who kept pushing me forward.

TABLE OF CONTENTS

LIST OF TABLES

LIST OF FIGURES

NOMENCLATURE

Abbreviations

B	Battery
EM	Electric Motor
F	Fuel
G	Generator
BSFC	Brake Specific Fuel Consumption
ICE	Internal Combustion Engine
MAP	Manifold Air Pressure
RPM	Revolutions per Minute
SOC	State of Charge
TAS	True Airspeed

Symbols

$\dot{m}$	Mass Flow Rate
η	Efficiency Ratio
ρ	Density
A	Ampere
C_D	Coefficient of Drag

C_L	Coefficient of Lift
C_P	Coefficient of Power
C_T	Coefficient of Thrust
D	Drag Force
g	Gravitational Constant of Earth
J	Propeller Advance Ratio
L	Lift Force
n	Rotational Speed
P	Pressure
S	Wing Reference Area
T	Thrust Force
W	Weight

Dynamics Variables

x	Horizontal Position
$\dot{x}$	Horizontal Velocity
$\ddot{x}$	Horizontal Acceleration
h	Vertical Position
$\dot{h}$	Vertical Velocity
$\ddot{h}$	Vertical Acceleration
V	Velocity Magnitude

Chapter 1

INTRODUCTION

The demand for air transportation is projected to increase dramatically, and with that comes an increase in the environmental impacts produced by air travel [1, 2]. To counter the environmental consequences associated with air travel, agencies around the world have established goals and research initiatives aimed at reducing the environmental footprint from aircraft. One of these efforts is led by the European Union Commission, whose Flightpath 2050 vision includes reducing aircraft CO_2 pollution by 75%, NO_x pollution by 90%, and reducing aircraft noise by 75% all by 2050 [3]. The International Air Transport Association also supports the reduction of carbon emissions with goals that call for a 1.5% average annual fuel efficiency improvement between 2010 and 2020, carbon neutral growth from 2020 onward, and a reduction of 50% in net emissions by 2050 compared to 2005 levels [4].

To meet the projected growth of air transportation while also improving environmental sustainability, the NASA Aeronautics Research Mission Directorate has set forth a vision for aeronautical research that focuses on efficient growth through the implementation of new technologies [5]. One of the priorities identified to realize these goals is an initiative to develop ultra-efficient subsonic transport through the use of alternative propulsion and energy. Key research themes to support the outcomes are ultra-efficient airframes, ultra-efficient propulsion, ultra-efficient vehicle system integration, as well as modelling, simulation, and testing capabilities.

Promising forms of alternative energy instead of gasoline are hydrogen fuel cells and electric batteries, but each form has its trade-offs in terms of energy and power per

mass and per volume. Hydrogen fuel cells have higher energy densities and specific energies compared to batteries, but batteries have higher power densities and specific power [6]. This means that when applied to a vehicle as a propulsion source, a hydrogen powered vehicle will generally have a high range and low power, and a battery powered vehicle will generally have a lower range but higher power output. For an aircraft, power is very important since takeoff and climb conditions require a large amount of power, but that power must come from an energy source that is low in weight and volume due to the very costly penalties that increasing weight and volume have on an aircraft. The combustion of fossil fuels such as an internal combustion engine combusting gasoline and a turbine combusting jet fuel offer this high power output from a fuel source that is relatively low in weight and volume, and has been the standard in aircraft propulsion since the beginning of powered flight. Combustion engines are not without drawbacks, however, and this combustion of fossil fuels produces emissions that are environmentally harmful.

In order to create a propulsion system that realizes the advantages of the different energy sources, multiple energy sources can be combined to form a hybrid propulsion system. In addition to reducing emissions, hybrid aircraft can also expand mission capabilities due to reduced thermal and acoustic signatures. The application of hybrid technology is already well established in the automotive industry, but it is an emerging practice in the aviation industry. One of the challenges in the development of hybrid aircraft is the feasibility of testing the aircraft, since there is a tremendous amount of time and money required to build a safe aircraft that meets regulations. Therefore, computational tools that can simulate the performance of a hybrid aircraft are incredibly useful in the design process.

Previous research on the simulation of hybrid aircraft has been conducted for a range of hybrid propulsion systems and airframes. On a small scale, a parallel hybrid propul-

sion system consisting of an internal combustion engine and battery was implemented into a 22 pound small unmanned aerial vehicle, with the combustion engine operating on a line of peak efficiency and charging the battery with excess power. Simulating the hybrid model over a defined flight mission achieved a fuel savings of 6.5% compared to the combustion engine only model [7]. Another study modelled a 227 pound single seat ultralight aircraft with a parallel internal combustion engine and battery in a MATLAB Simulink and X-Plane environment that allowed for real time simulations, and found fuel savings of up to 31.1% compared to the standard combustion engine only model [8]. In another study, a Cirrus SR20 with a combustion engine and battery in a parallel hybrid configuration was simulated and compared to flight test data to demonstrate a fuel savings of 15.6% compared to the standard SR20 [9].

The limitation of this previous research is that the results are specific to one configuration of a hybrid aircraft. There are a myriad of hybrid combinations, though, based on different types of hybrid architectures as well as the individual components that make up a hybrid propulsion system. This presents a challenge when designing a hybrid aircraft, since the vastness of the design space means that there are a seemingly limitless amount of configurations for which it would be difficult to effectively explore the solutions. In order to more effectively explore the diverse design space of hybrid aircraft, this thesis proposes a simulation tool that is not specific to one design, but capable of being easily configurable for different hybrid architectures and components.

1.1 Hybrid Aircraft Types

A hybrid propulsion system is one that consists of two different energy sources, which for aircraft is typically a thermal or electrochemical machine and electric machine.

The electric machine is comprised of a battery and electric motor, and the thermal or electrochemical machine can be an internal combustion engine, gas turbine engine, or a hydrogen fuel cell. No matter what energy sources are used, though, the end result is to produce power to spin a propeller or turbine to create thrust to propel the aircraft. This flow of power from the energy source to the propeller or turbine can be done in a variety of ways depending on how the components of the hybrid propulsion system are arranged. The three most common configurations, known as a series hybrid, parallel hybrid, and series-parallel hybrid are discussed next.

A series hybrid propulsion system has the configuration shown in the block diagram in Figure 1.1, and is considered the most simple hybrid system. In the series hybrid, the propeller or turbine is only driven by the electric motor, and the thermal machine is mechanically decoupled from the load which means that it can operate at speeds and torques in its region of high efficiency [10]. A disadvantage of the series hybrid is that the mechanical power from the thermal machine has to be transformed twice, since it's first converted to electrical power through the generator and then back to mechanical power through the electric motor, and this requirement of a generator also means added weight [11]. The electrical power from the generator can either be used to drive the electric motor, or during phases of flight when low power is required the excess generated power can be used to charge the battery.

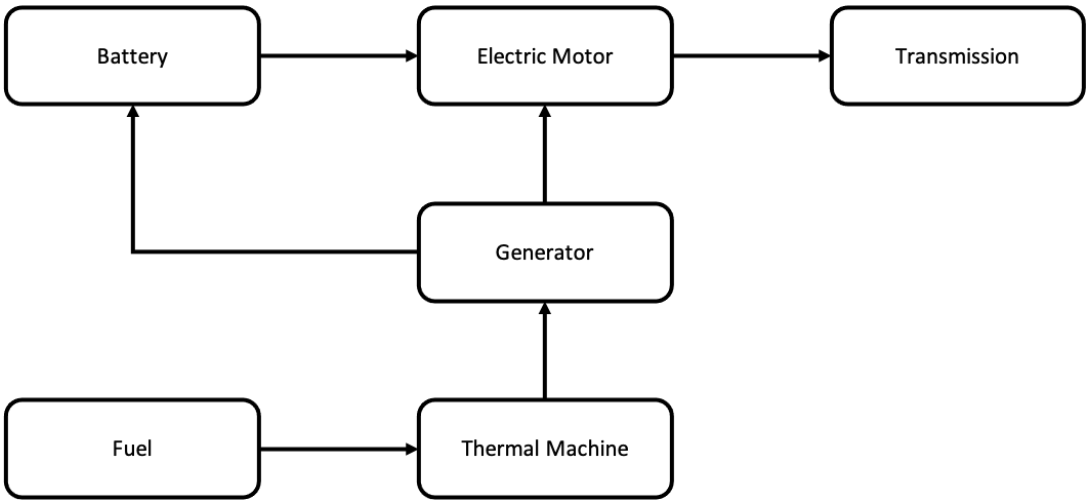

Figure 1.1: Block Diagram of Series Hybrid

A parallel hybrid scheme is shown in Figure 1.2. Compared to the series hybrid, in a parallel hybrid the electric machine and thermal machine are both connected to the propeller or turbine drivetrain. In this way power can be supplied by the electric motor alone, the thermal machine alone, or both the electric motor and thermal machine at the same time. Since the thermal machine is directly connected to the drivetrain, this eliminates the need for a generator [10]. Another advantage is that a less powerful electric motor and thermal machine can be used to deliver the same rated power as a series hybrid [12]. The disadvantages of a parallel hybrid are the added complexity from a transmission system so that the electric machine and thermal machine can be coupled and decoupled from the drivetrain, and that the thermal machine cannot operate in its high efficiency region at all times since it is mechanically coupled to the load [13, 10]. The battery can still be charged in a parallel hybrid when the thermal machine produces excess power and the electric motor acts as a generator to turn that excess mechanical power into electrical power to charge the battery.

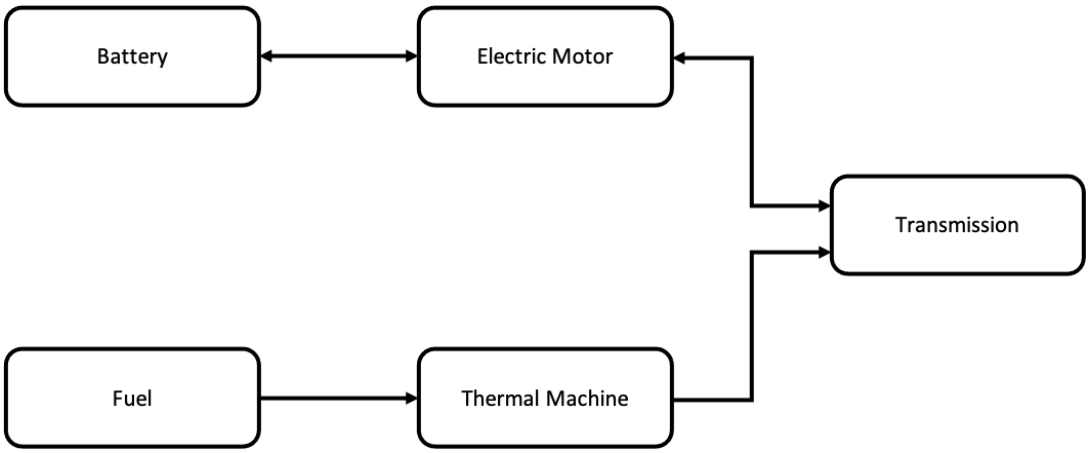

Figure 1.2: Block Diagram of Parallel Hybrid

A series-parallel hybrid propulsion system, diagrammed in Figure 1.3, is another option that combines the features of both the series and parallel hybrid. It has the advantage of the electric motor and thermal machine both being able to deliver power together or separately to the propeller or turbine drivetrain, and the thermal machine can also work in its region of peak efficiency [10]. Although it has the advantages of the series and parallel hybrid, it is more complicated to control both in simulation and for a real system since a series-parallel hybrid has more ways it can be operated [13]. For example, the power from the thermal machine can either be sent directly to the drivetrain, or converted to electrical power through the generator and used to charge the battery or drive the electric motor, so establishing this control logic becomes a complex task.

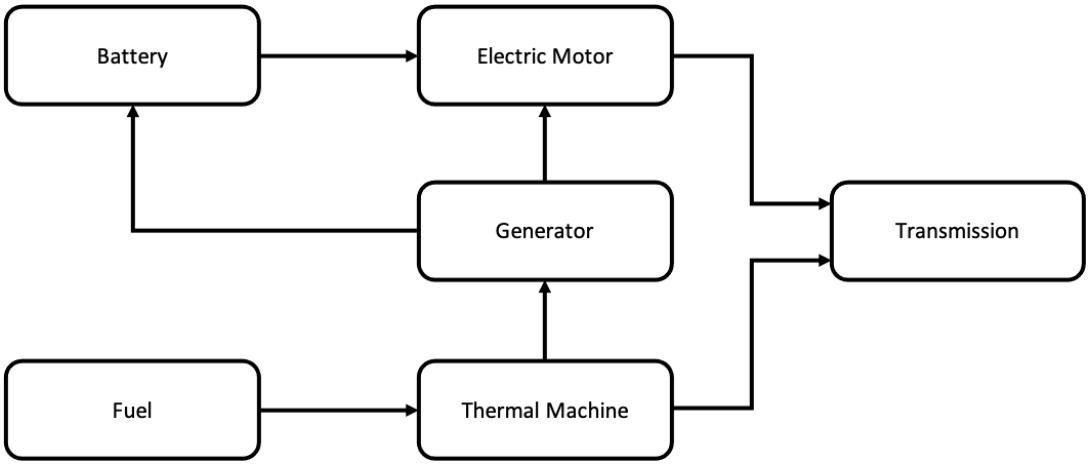

Figure 1.3: Block Diagram of Series-Parallel Hybrid

1.2 Project Scope and Goals

The goals of this thesis align with key research themes identified by NASA to develop more efficient aircraft, namely research on ultra-efficient propulsion, ultra-efficient vehicle system integration, as well as modelling, simulation, and testing capabilities [5]. With a configurable hybrid aircraft simulator, these more efficient propulsion sources can be explored and integrated into a vehicle level system and optimized for goals such as minimizing fuel consumption. To streamline the complementary processes of modelling, simulation, and testing, this thesis was developed in conjunction with NASA Grant 80NSSC20K0493 that is enabling the construction a hybrid aircraft test bed, which creates a direct link for test data to be used in the model creation process and further simulation validation.

Based on the research demands and project goals previously discussed, this thesis focuses on simulating the performance of a hybrid aircraft with an emphasis on being easily configurable for different types of hybrid structures and hybrid propulsion system components. Whether a series, parallel, or series-parallel hybrid type is selected, the components of the hybrid propulsion system can be arranged in a manner con-

sistent with the block diagrams in Figures 1.1-1.3 to create the desired hybrid type. Additionally, once a hybrid structure is set, it is simple to change a component of the hybrid propulsion system to evaluate the system and vehicle level effects that any component has.

First, in Chapter 2, a general simulation framework is established that supports the modularity of the hybrid aircraft model and so that the simulator maintains proper functionality for any hybrid configuration. The framework is broken down into subsystems that represent the aircraft dynamics, controls, aerodynamic properties, as well as the hybrid propulsion system, and the requirements that ensure seamless configuration changes are discussed. In Chapter 3, the methodology for creating a model of each hybrid propulsion system component is examined so that the simulator can support the many different hybrid components available to the user. Next in Chapter 4, the simulator is validated using flight test data of a non-hybrid aircraft to demonstrate that the performance of the simulated aircraft is representative of a real aircraft, and that the control strategy is capable of keeping the aircraft on a given flight profile. Finally, in Chapter 5, this thesis includes an example of modelling a hybrid aircraft and simulating it over different flight profiles in order to study the performance of the hybrid propulsion system, including trends in fuel consumption.

Chapter 2

SIMULATOR FRAMEWORK

As mentioned in the scope of this project, there is a focus on making this hybrid aircraft simulator configurable for different types of hybrid architectures as well as different hybrid components. Therefore, a general framework for the simulator needs to be established so that the simulator will function correctly for any hybrid configuration. This chapter will discuss the simulator framework that supports this goal. First, the dynamics and controls of the simulator will be discussed to give context to how the hybrid propulsion system is implemented into the simulator framework. Then, the methodology of modelling each component in the hybrid propulsion system will be explored. Throughout the chapter, the inputs and outputs of pieces in the framework will be defined so that all the elements of the simulator can work together to ensure seamless configuration changes of the hybrid system.

2.1 Simulator Overview

The main goal is to simulate the performance of a hybrid aircraft using a framework that allows for the implementation of the wide range of hybrid types and components available. Key results of the simulator are performance parameters such as the speed and altitude, along with metrics about the hybrid propulsion system, which the user can exploit for design and optimization such as minimizing fuel consumption. Since it's desirable to create a simulator framework that is capable of handling different hybrid aircraft configurations, certain input and output relations have to be defined in such a way that changes to the hybrid system can be made without breaking

the functionality of the overall simulator framework. The simulator built for testing and producing results for this project was made using MATLAB Simulink, however, the methodology in this chapter is presented in a way to be implemented in other programming environments.

As seen in Figure 2.1, the simulator framework is broken down into blocks that contain the aircraft dynamics, controls, aerodynamic properties, and hybrid propulsion system. The arrows represent specific inputs and outputs that are required for the simulator to function properly. These blocks and their required inputs and outputs are a minimum configuration of the framework, meaning that the simulator will not run without them but that more parameters can be added if desired by the user. For example, the hybrid propulsion system block in Figure 2.1 contains details such as the power distribution between the generator and battery which are useful parameters to the user in assessing the performance of the hybrid system, but are not parameters that the framework is dependent on. The following sections will discuss these necessary inputs and outputs for each block, along with the internal details, that assemble a functional framework.

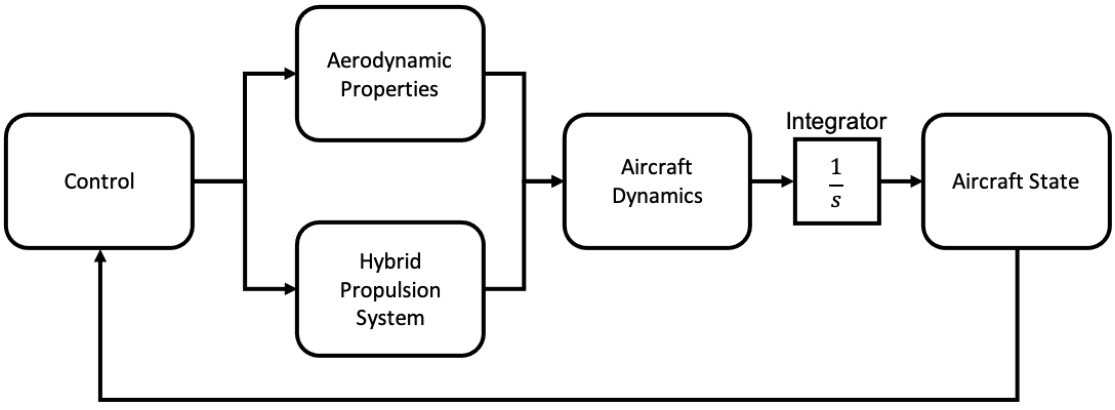

Figure 2.1: Block Diagram of Hybrid Aircraft Simulator

2.2 Aircraft Dynamics

The aircraft dynamics block contains the state-space equations which mathematically model the motion of the physical aircraft. The aircraft state at each timestep is determined by integrating the outputs of the state-space equations, which depend on the input variables of lift, drag, thrust, and weight forces acting on the aircraft. This section discusses the dynamics model of the aircraft including the derivation of the state-space equations and calculations of the input variables.

With the purposes of this project being to simulate performance metrics such as the speed and altitude, it is appropriate to model the aircraft as a point mass. The pitch dynamics cannot be simulated since a point mass model does not consider the moments of inertia of the aircraft, but that is not relevant to the desired performance results and metrics about the hybrid propulsion system. The free body diagram in Figure 2.2 shows the aircraft represented as a point mass and the forces that act on it. As depicted in the figure, the point mass model assumes all forces act on the center of gravity of the aircraft. This free body diagram is the first step in deriving the state-space equations, and the forces included need to be known to solve the state-space equations.

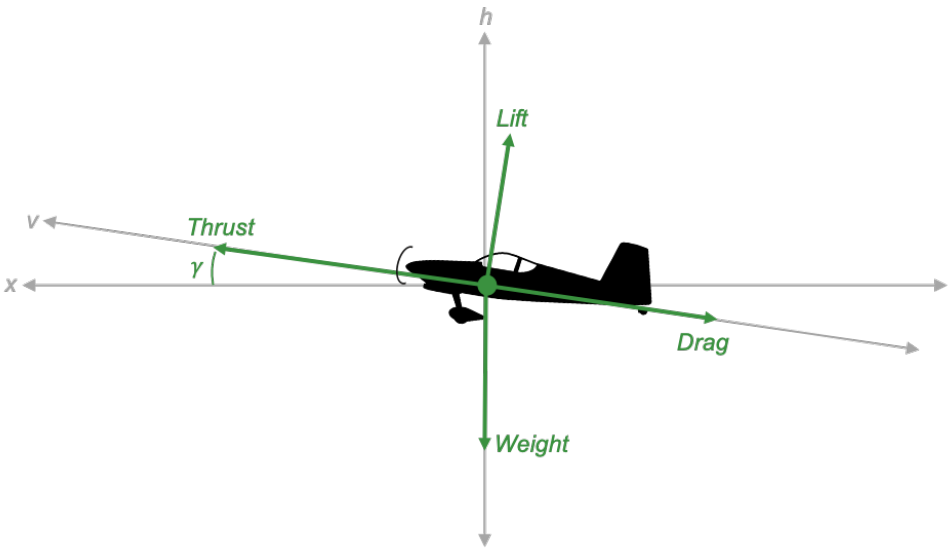

Figure 2.2: Free Body Diagram

In Figure 2.2, the x axis is horizontal and the positive direction forward, the h axis is vertical and the positive direction upward, and the v axis is in the direction of the trajectory of the aircraft. The lift force acts normal to the trajectory of the aircraft, and the thrust and drag forces act in line with the trajectory of the aircraft. The weight force always acts down in the negative h direction. Since the aircraft will only be simulated at small angles of attack, it is assumed that the trajectory angle, γ, is equal to the pitch angle of the aircraft.

From the free body diagram in Figure 2.2, the equations for the acceleration of the aircraft can be expressed in terms of the acting forces and the mass or weight of the aircraft. The acceleration in the horizontal and vertical directions are as follows:

$$\ddot{x} = \frac{g}{W}[Tcos(\gamma) - Dcos(\gamma) - Lsin(\gamma)] \tag{2.1}$$

$$\ddot{h} = \frac{g}{W}[Lcos(\gamma) + Tsin(\gamma) - Dsin(\gamma) - W] \tag{2.2}$$

A third differential equation is needed to find the weight of the aircraft since it changes as fuel is burned.

$$\dot{W} = -\dot{m}_F \tag{2.3}$$

These differential equations are useful in defining the state-space equations, which must be expressed as first-order equations in order to be integrated as an initial value problem. It is convenient to use the following state variables:

$$\begin{aligned} s_1 &= x \\ s_2 &= \dot{x} \\ s_3 &= h \\ s_4 &= \dot{h} \\ s_5 &= W \end{aligned} \tag{2.4}$$

Taking the derivative of the state variables leads to the following state-space equations:

$$\begin{aligned} \dot{s_1} &= s_2 \\ \dot{s_2} &= \tfrac{g}{W}[Tcos(\gamma) - Dcos(\gamma) - Lsin(\gamma)] \\ \dot{s_3} &= s_4 \\ \dot{s_4} &= \tfrac{g}{W}[Lcos(\gamma) + Tsin(\gamma) - Dsin(\gamma) - W] \\ \dot{s_5} &= -\dot{m}_F \end{aligned} \tag{2.5}$$

The forces that show up in the state-space equations are not directly known and can be solved for using the following equations:

$$V = \sqrt{\dot{x}^2 + \dot{y}^2} \tag{2.6}$$

$$\gamma = tan^{-1}\left(\frac{\dot{h}}{\dot{x}}\right) \tag{2.7}$$

$$L = \frac{1}{2}\rho(h)V^2SC_L \tag{2.8}$$

$$D = \frac{1}{2}\rho(h)V^2 S C_D(C_L) \tag{2.9}$$

While not required to solve the state-space equations, the weight of fuel consumed can be an output variable that is useful in analyzing the performance of the hybrid propulsion system. It is calculated by the following equation:

$$W_F = W_{initial} - W \tag{2.10}$$

Numerically integrating the above state-space equations in Equation 2.5 yield the state variables in Equation 2.4 for the current timestep. Equation 2.6 represents the true airspeed of the aircraft assuming no winds, but wind effects can be included by including the wind speed in the x or h direction. The true airspeed is the speed of the aircraft relative to the air it's flying through, and is used in aerodynamic calculations such as the lift and drag forces calculated in Equations 2.8 and 2.9. The S variable is the wing reference area of the aircraft, which is constant. The air density, ρ, is not constant and depends on the altitude, h. The $\dot{m}_F$ variable is the rate of fuel being consumed by the thermal machine, so it is a necessary input variable.

The control variables of the state-space equations from Equation 2.5 are the thrust force and lift coefficient, which are related to how a real aircraft is controlled. To control the speed and altitude of a real aircraft a pilot uses the stick or yoke to deflect the elevator, and the throttle to adjust the power. Deflecting the elevator changes the pitch moment, which changes the angle of attack and thus the lift produced. Adjusting the throttle controls the engine power and propeller speed, effectively changing the thrust produced by the propeller. The next section will discuss the control mechanisms in place that regulate the control variables of thrust force and lift coefficient.

2.3 Feedback Control

The simulator uses closed-loop control to regulate the control variables based on feedback from the aircraft state and information from the user. This is accomplished through the use of PID control, diagrammed in Figure 2.3, which is a form of control loop feedback that produces an output based on a calculated error between a setpoint and a measured value. A PID controller itself contains the proportional, integral, and derivative terms defined in Figure 2.3 that are applied to the error in order to create a control action.

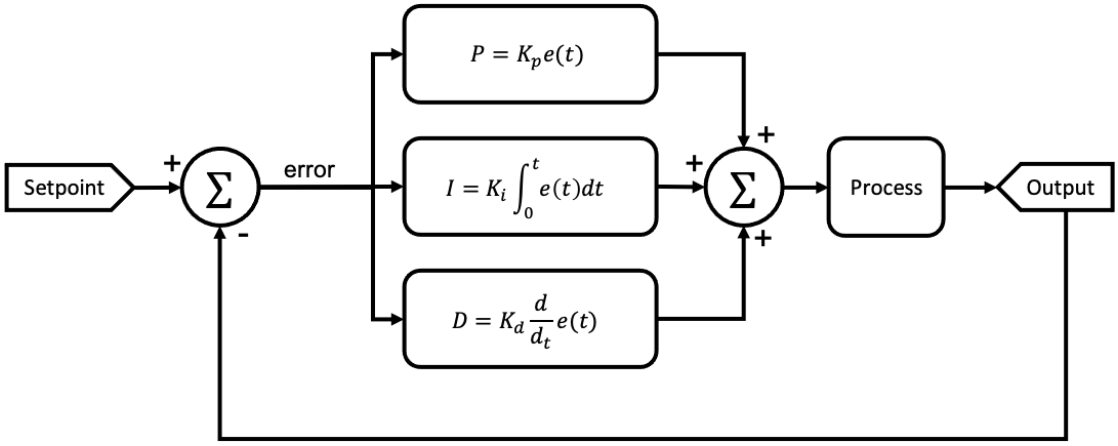

Figure 2.3: Block Diagram of PID Control

The simulator has two PID controllers, one for controlling the lift coefficient of the aircraft and another for controlling the thrust produced. The output of the lift coefficient PID controller can be the lift coefficient itself, but the output of the thrust PID controller is some variable that is an input to the hybrid propulsion system that controls the amount of thrust produced. This could be a thrust command, but it could also be other variables such as a torque command for the electric motor, manifold pressure for the internal combustion engine, or throttle setting for the internal combustion engine for example.

There are two strategies for controlling the speed and altitude of the aircraft through the PID controllers, though. One is that the lift coefficient controls the speed and the thrust controls the altitude. The second is that the lift coefficient controls the altitude and the thrust controls the speed. This section will discuss which strategy results in better control of the aircraft and expand on the details of the PID controllers.

2.3.1 Speed and Altitude Control

To determine which of the two control strategies as described above results in better control of the aircraft, simulations were run for a conventional combustion engine aircraft using both cases. The setpoints for the speed and altitude were speed and altitude measurements from a flight test of that aircraft which varied in both speed and altitude in order to observe differences between the two control strategies during dynamic behavior of the aircraft. Results of the speed and altitude of the simulated aircraft compared to the speed and and altitude setpoints are shown for both control strategies, with Figures 2.4 and 2.5 showing the results of controlling the speed with the lift coefficient and the altitude with the thrust.

The altitude and speed error plotted are also the error terms for the PID controllers, as depicted in Figure 2.3. Both the simulated speed and altitude track the profile well, with the altitude error being a maximum of 24 feet and the speed error being a maximum of about one mile per hour. Note that the speed and altitude measurements from the flight test contain noise, so the setpoints are not a smooth profile which contributes to the smaller oscillatory error values. It is maximum error values and the divergence patterns of the error that are of more importance in comparing the two control strategies.

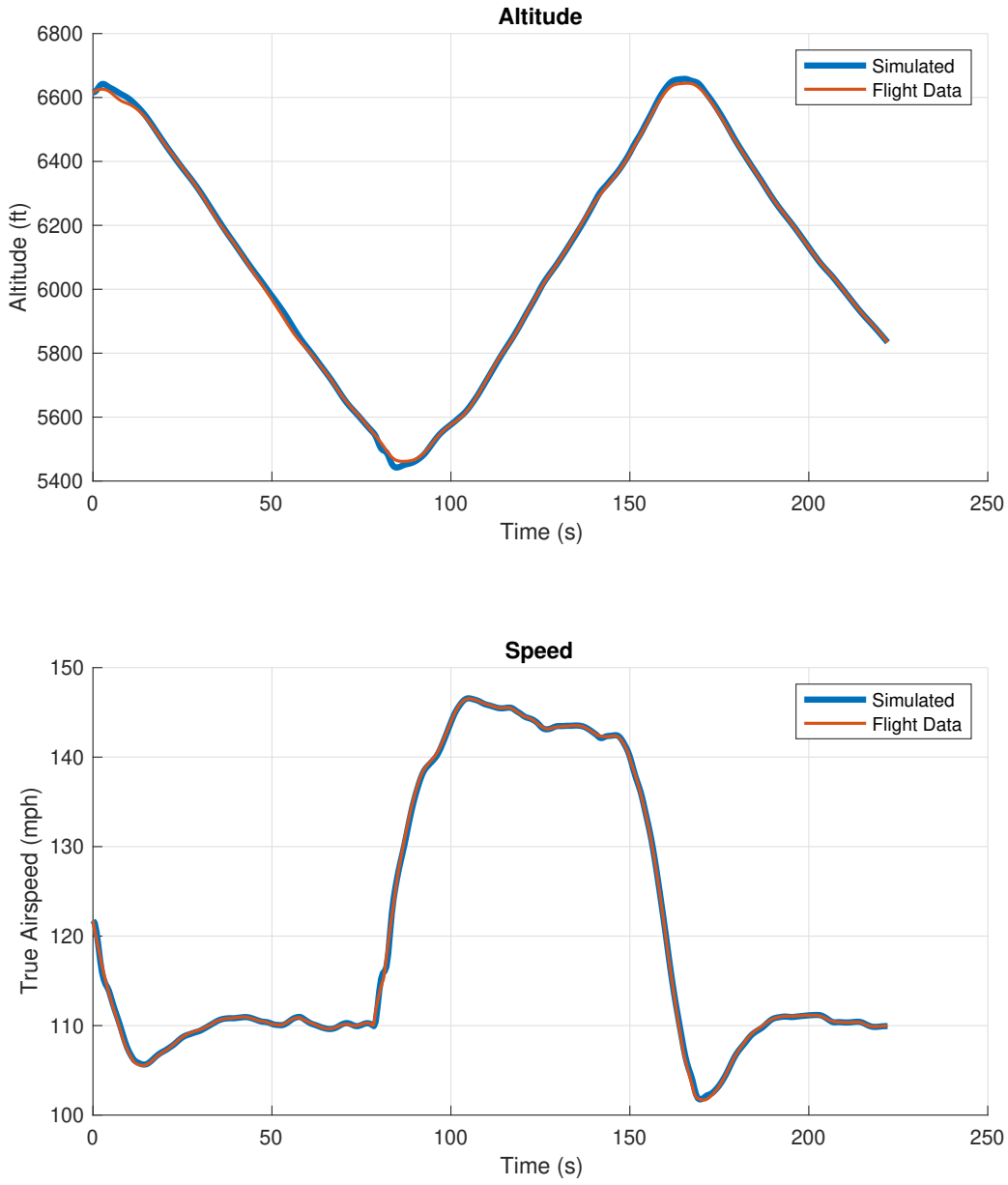

Figure 2.4: Thrust Controls Altitude and Lift Controls Speed Results

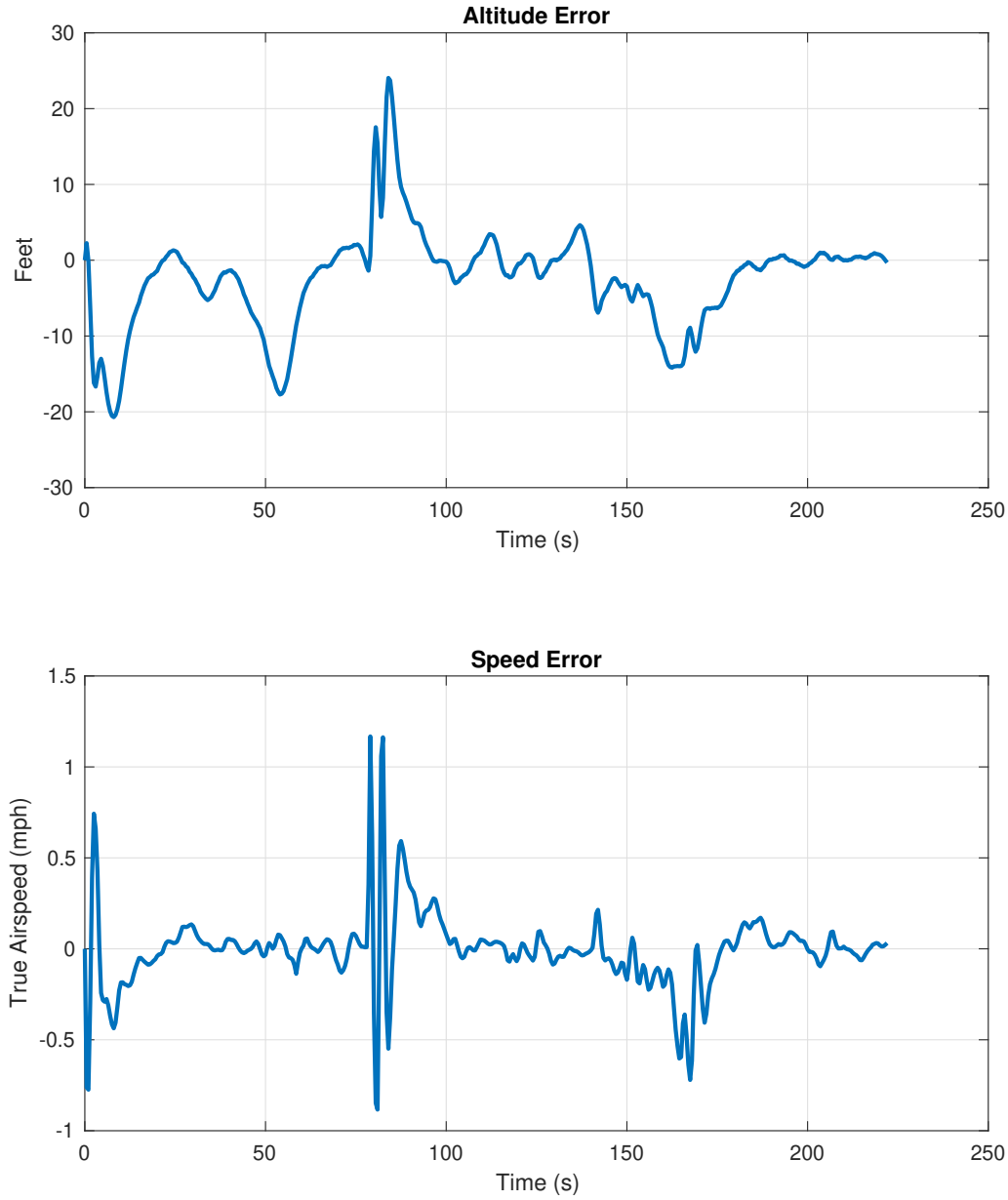

Figure 2.5: Thrust Controls Altitude and Lift Controls Speed Errors

Figures 2.6 and 2.7 are the results of controlling the speed with the thrust and the altitude with the lift coefficient. The simulated altitude matches the altitude profile well, but it is apparent that the simulated aircraft speed poorly tracks the speed profile. The altitude error is actually reduced for this strategy, with a maximum error of about 3 feet, however, the speed error increases to about 17 miles per hour.

Looking at Figure 2.6, it is apparent that the speed error is the largest when the altitude setpoint profile begins a steep climb. Under this control strategy where the lift coefficient controls altitude, the lift coefficient is increased to initiate the climb, which causes a reduction in speed. The engine power is then increased to increase the speed, but due to the steepness of the climb angle, the aircraft cannot accelerate when climbing even though the engine is operating at maximum power. In contrast, when altitude is controlled by thrust, the climb is initiated by increasing power and the speed does not decrease when entering a steep climb as in Figure 2.4.

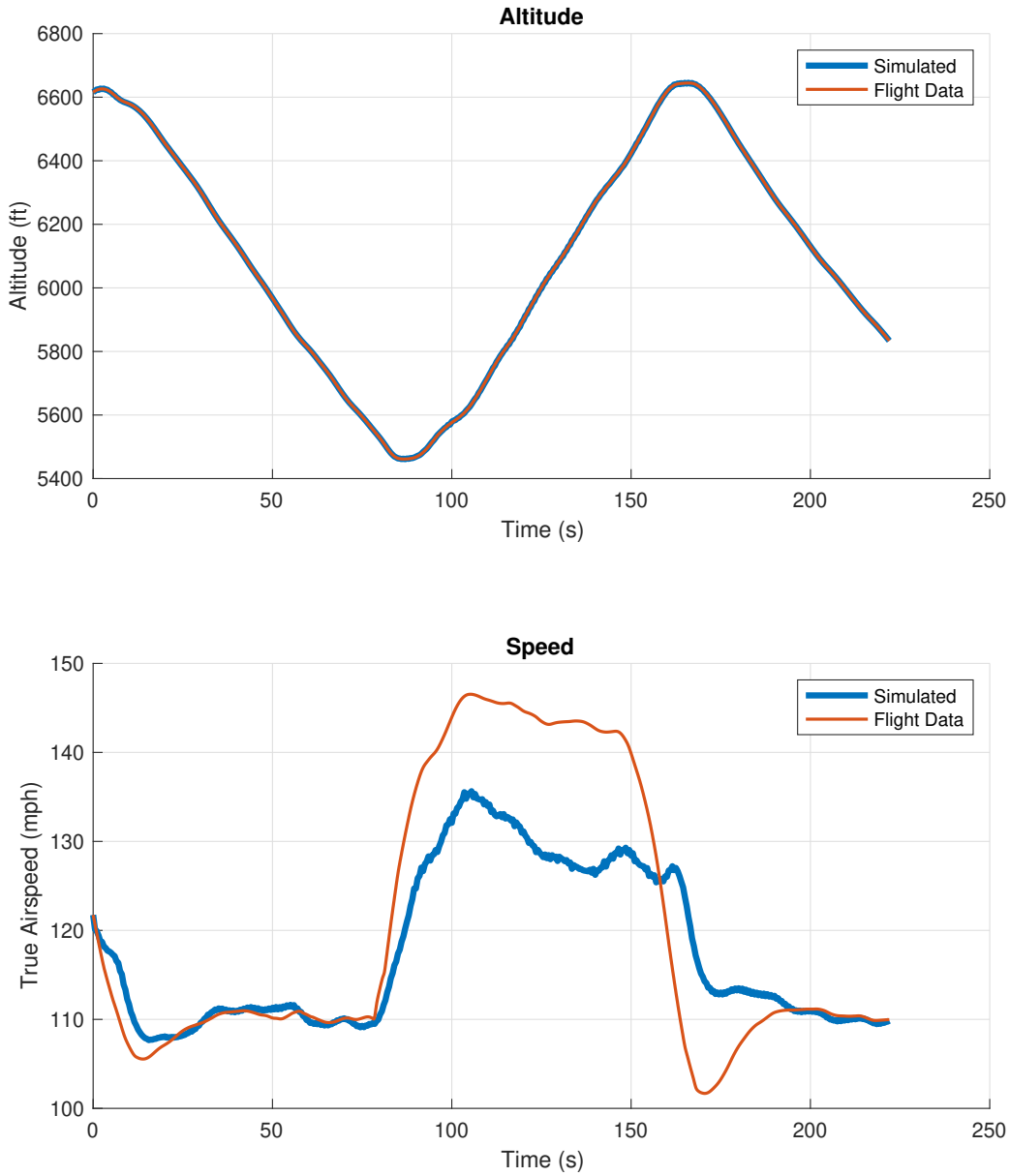

Figure 2.6: Lift Controls Altitude and Thrust Controls Speed Results

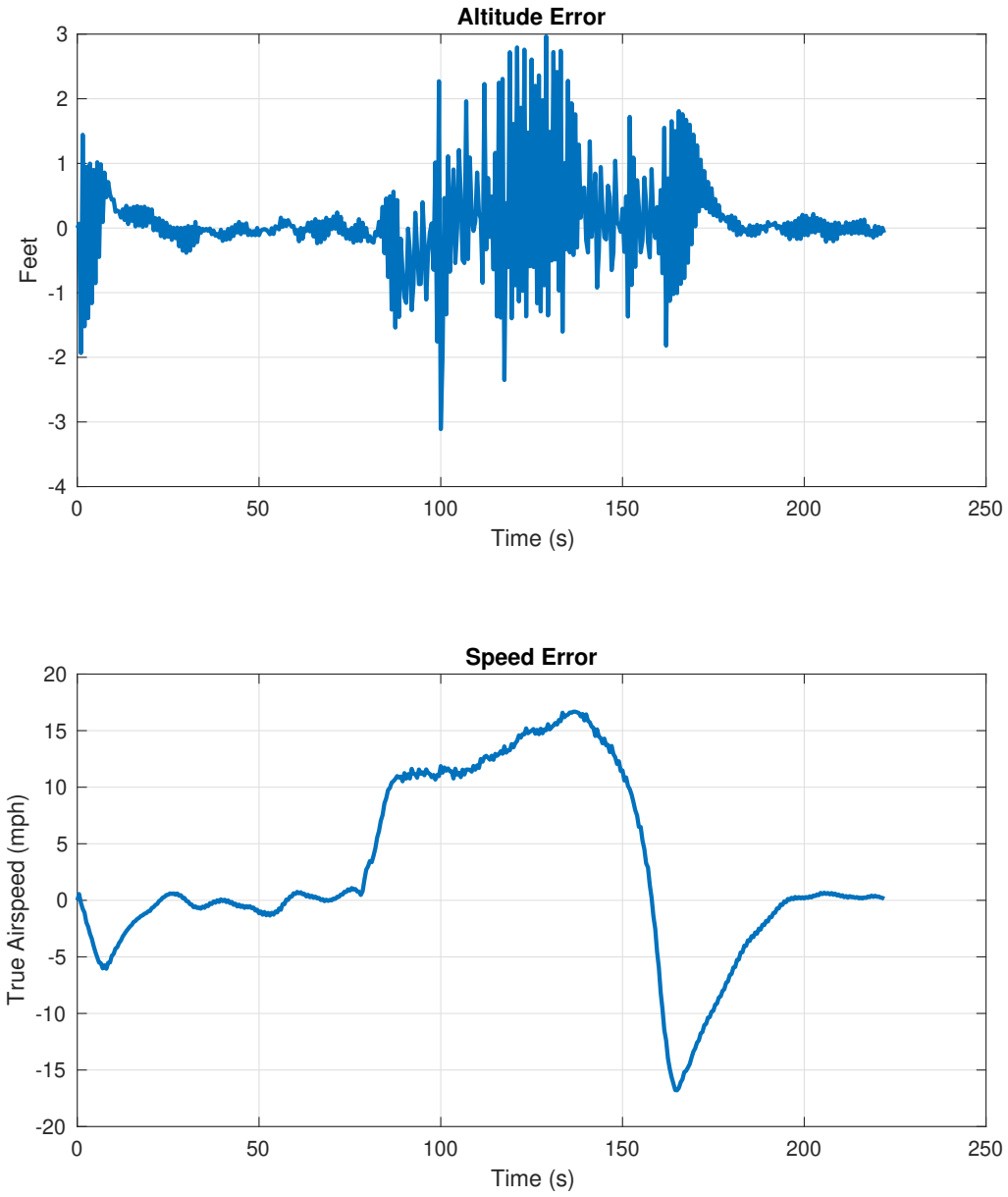

Figure 2.7: Lift Controls Altitude and Thrust Controls Speed Errors

One of the important factors of the PID control to analyze is the ability to eliminate steady-state error. By looking at the speed and altitude errors of the first control strategy in Figure 2.5, it can be seen that when the error increases the PID control is able to control the aircraft in such a way to reduce the error. In contrast, by looking at the speed error of the second control strategy in Figure 2.7, there are long time periods when the error is relatively large and not being reduced indicating that

the steady-state error is not being eliminated in a timely manner. Furthermore, the results of these simulations reveal that changing the lift coefficient produces faster and more responsive changes to the speed or altitude it is controlling compared to changing the thrust control variable. The error is also lower for whichever parameter is controlled by the lift coefficient.

These results and observations lead to the first control strategy of the PID controlled lift coefficient controlling the speed and the PID controlled thrust variable controlling altitude to be the more optimal method for controlling the aircraft. The worst error from that strategy of about 24 feet of altitude is certainly better than the 17 miles per hour error in speed that resulted from using the other control strategy, since the performance of the hybrid propulsion system is more affected by the speed of the aircraft compared to the altitude. A difference of 20 miles per hour results in a significantly different amount of power required by the propulsion system, but a difference of 20 feet in altitude is a negligible change in air density. Additionally, the chosen control method results in the PID controllers being more effective in reducing the steady-state error.

2.3.2 Flight Path Input

Error values processed by a PID controller, such as in Figure 2.3, are the difference between a measured value of the aircraft state and a setpoint value which is provided by the user. For this simulator, the user can input the setpoints in the form of a speed and altitude profile defined over a set time. Making a speed and altitude profile is a convenient way for the user to control the flight path of the simulated aircraft since it is easier to visualize a flight path in terms of speed and altitude rather than power and elevator deflection angle, for example. The difference between the speed setpoint from the profile and the simulated speed of the aircraft is the error that is input to

the speed PID controller that outputs a lift coefficient, and the difference between the altitude setpoint from the profile and the simulated altitude of the aircraft is the error that is input to the altitude PID controller that outputs a thrust control action.

Other parameters can be used to define the speed and altitude as well, since the simulator framework is designed to be flexible and not constrain the user. For example, rather than specify an altitude profile, the user can create a power profile that specifies the desired power produced by the hybrid propulsion system. The error between the desired power and actual power produced will be the input to the altitude PID controller and the thrust control output will control the hybrid propulsion system in a manner that minimizes the difference between the desired power and actual power. Note that when using input profiles other than speed and altitude, the simulated aircraft is no longer constrained to a certain flight path trajectory. For instance, defining a profile that is a high speed and low power could result in the aircraft rapidly descending toward the ground to pick up speed as there is not enough power to maintain that speed at a steady altitude. However, the ability to input profiles other than speed and altitude profiles can be useful for optimization techniques.

2.4 Aerodynamic Properties

As presented in Equation 2.9, the drag coefficient is a function of the lift coefficient. This functional relationship is contained within the aerodynamic properties block of the framework and requires the input to be the lift coefficient and the output to be the drag coefficient. This is convenient because the drag polar of an aircraft is a curve of lift coefficient versus drag coefficient that essentially quantifies the amount of drag produced by the aircraft in relation to how much lift is being generated. Typically a drag polar is generated for steady flight, which is suitable for this application since

the expected simulations are not highly dynamic in terms of rapidly changing angles of attack.

There are a variety of ways to express the drag polar of the aircraft within the aerodynamic properties block, one example being to interpolate tabulated data. If drag coefficients are tabulated for corresponding lift coefficients, the drag coefficient can be interpolated based on the lift coefficient input. Another option is expressing the drag coefficient as an equation that is only dependent on the lift coefficient input. Oftentimes drag polars are expressed as a more simple parabolic function, but it is not required to be parabolic as long as it only depends on the lift coefficient. A drag polar is also common information known about real aircraft through flight testing or conceptual aircraft design through estimation methods, so it is easy to implement into the simulator [14, 15, 16, 17].

2.5 Hybrid Propulsion System

The block diagram of the hybrid propulsion system in Figure 2.8 indicates the components contained in the system which include a propeller, electric motor, generator, internal combustion engine, and battery. As mentioned previously, it is important for any configuration of the hybrid propulsion system to work with the rest of the simulator framework. No matter what hybrid architecture or components are used, there is a minimum configuration of inputs and outputs as referenced in Figure 2.8.

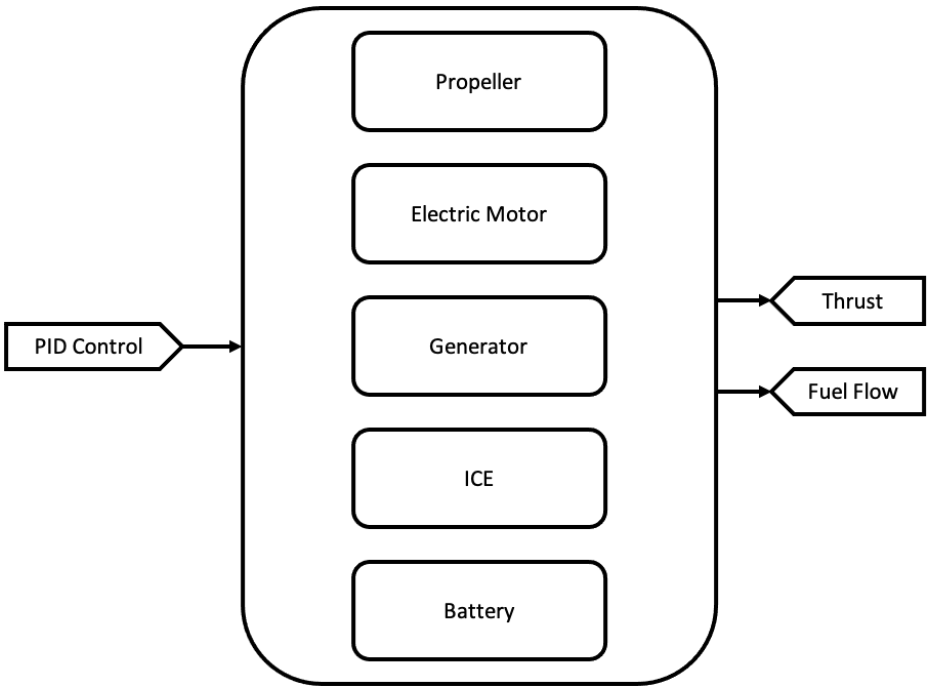

Figure 2.8: Block Diagram of Hybrid Propulsion System

In order to properly integrate the hybrid propulsion system into the simulator framework, a required input must be the thrust control action from the altitude PID controller. As mentioned in the controls section, this can be any variable that controls the thrust such as a torque command, throttle position, or manifold pressure for example. The outputs of the hybrid propulsion system must contain the thrust force and fuel flow, since the thrust force and fuel flow are both required to solve the state-space equations described in Equation 2.5. Note that as described in Section 2.2, the thrust force is a control variable to the state-space equations and therefore has a large influence on the behavior of the aircraft. The fuel flow is used in calculating the aircraft weight and the amount of fuel burned, which is an important performance metric.

The blocks representing the hybrid component models in Figure 2.8 can be connected in a number of ways based on the different hybrid architecture options as outlined

in Section 1.1. For example, a series hybrid like in Figure 1.1 will have the propeller connected to the electric motor which is receiving power from the battery and generator. Or a parallel hybrid, such as in Figure 1.2, can have both an electric motor and internal combustion engine connected to the propeller through a clutch and gearbox. Once a hybrid architecture type is set, the models of each component can also be changed without having to adjust the framework. For instance, if the user decides to select a different electric motor, it is as simple as switching the electric motor block. To achieve this level of component and connective modularity, though, the models of each component must follow specific inputs and outputs. This section will describe these required inputs and outputs for each component in the hybrid propulsion system.

2.5.1 Propeller

An aircraft propeller converts mechanical shaft power into a thrust force that propels the aircraft forward. Propeller blades are airfoil shaped, and this shape combined with the angular velocity of the propeller accelerate the air passing through the propeller region. The propeller model is defined by the inputs and outputs listed in Table 2.1.

Table 2.1: Propeller Model Inputs and Outputs

Input	RPM	Propeller rotational speed
Input	V	True airspeed
Input	ρ	Air density
Output	$Thrust$	Thrust produced
Output	$Power_P$	Propeller power required

The propeller model is set up to find the thrust coefficient and power coefficient of the propeller based on an advance ratio, which is convenient because that data is commonly provided by the propeller manufacturer or found through blade element momentum theory software [18, 19]. This is achieved by interpolating the coefficient

of thrust and power data based on a given advance ratio. The propeller efficiency can also be interpolated from the advance ratio, and while not required to run the simulation, the propeller efficiency can be a useful performance metric.

The advance ratio at the current timestep needs to be known in order to interpolate the propeller data. Advance ratio is defined in Equation 2.11, where the advance ratio, J, depends on the true airspeed, V, the propeller rotational speed, n, and the propeller diameter, D.

$$J = \frac{V}{nD} \tag{2.11}$$

Knowing the advance ratio, the coefficient of thrust, C_T, and coefficient of power, C_P, can be interpolated from the propeller data. Once the coefficients are determined, the thrust force is calculated by Equation 2.12.

$$T = C_T \rho n^2 D^4 \tag{2.12}$$

The power produced by the propeller is calculated by Equation 2.13.

$$Power_P = C_P \rho n^3 D^5 \tag{2.13}$$

This $Thrust$ output is the control variable input to the state-space equations of the aircraft dynamics model. The output, $Power_P$, is used in matching the power of the propeller and the power of whichever other components are directly driving the propeller, such as an electric motor or internal combustion engine.

2.5.2 Electric Motor

An electric motor converts electric power to mechanical shaft power. The most important metric of an electric motor is the efficiency ratio of output to input power

[20]. The efficiency ratio is not a constant and changes with the motor speed and torque, so it is necessary for the electric motor model to account for the efficiency ratio across all operating conditions. The electric motor model function is defined by the following inputs and outputs in Table 2.2.

Table 2.2: Electric Motor Model Inputs and Outputs

Input	RPM	Motor rotational speed
Input	$Torque$	Torque command
Output	$Power_{EM}$	Motor power produced
Output	$Current_{EM}$	Current required by motor

The electric motor model is based on efficiency data commonly provided by the electric motor manufacturer. An efficiency map, such as in Figure 2.9, is a contour plot that gives the motor efficiency for the range of motor speeds and torques. An efficiency map such as this can be digitized to collect data points, or tabulated data can be used if provided.

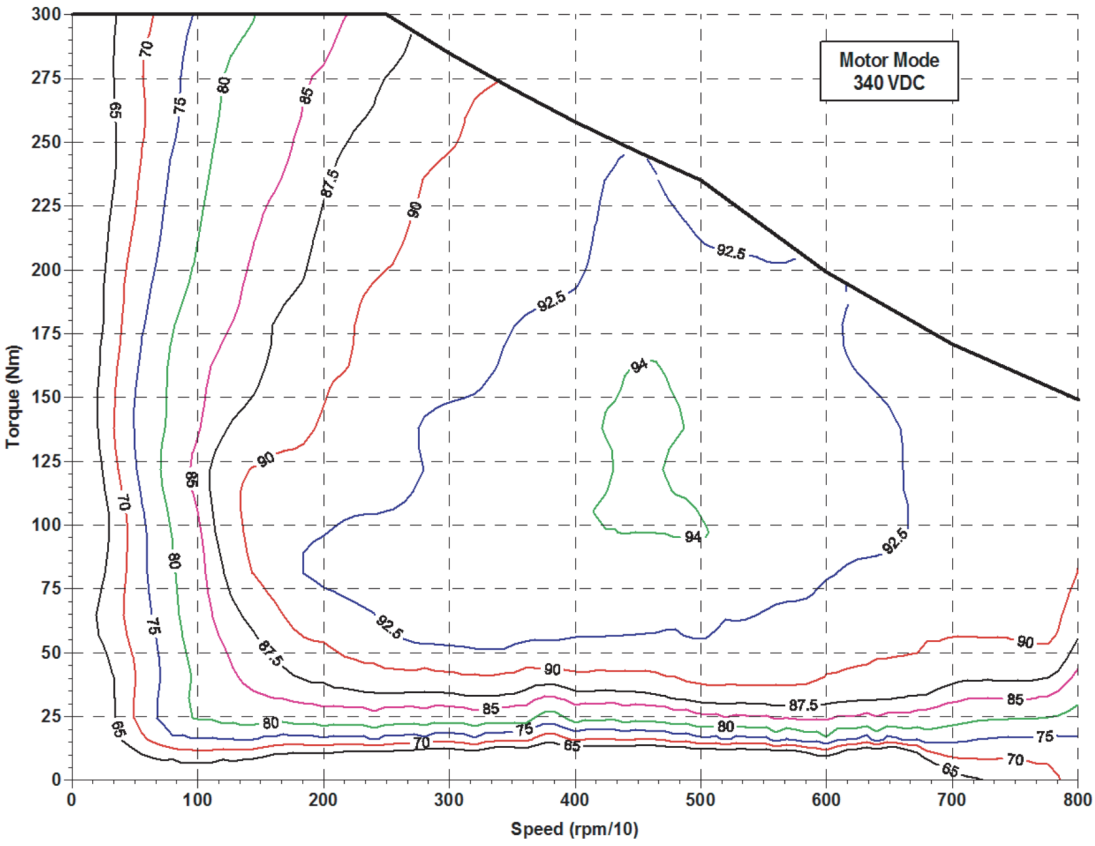

Figure 2.9: Efficiency Map of Electric Motor [21]

The electric motor model function uses the RPM and $Torque$ inputs to do a 2D interpolation of the efficiency data to estimate the motor efficiency at the given motor speed and torque. This efficiency is then used to determine the current required by the motor. Since there is a loss associated with the electric motor converting the electric power to mechanical power, this needs to be reflected in the model. The mechanical power produced is simply the product of the motor speed and commanded torque, as calculated in Equation 2.14, and the current required by the electric motor to produce that power is calculated by Equation 2.15.

$$Power_{EM} = RPM \cdot Torque \tag{2.14}$$

$$Current_{EM} = \frac{Power_{EM}}{Voltage \cdot \eta_{EM}} \tag{2.15}$$

The efficiency ratio, η_{EM}, is not required to be an output of the model, but it can be a useful performance metric for optimization since it is desirable to minimize the power losses. Electric motors are also designed to work at a nominal voltage, which needs to be specified in the model to calculate the current required.

2.5.3 Generator

A generator is essentially the opposite of an electric motor and converts mechanical shaft power into electrical power, in fact, some electric motors can also be used as generators [22]. Like an electric motor, there is a power loss quantified by the efficiency ratio. The generator model is defined in Table 2.3, and is similar to the electric motor model in terms of inputs and outputs.

Table 2.3: Generator Model Inputs and Outputs

Input	RPM	Generator rotational speed
Input	$Torque$	Torque applied
Output	$Current_G$	Current produced by generator

The data required for the generator model is the same as the electric motor model, which are the efficiencies associated with a range of rotational speeds and torques. It is common for the generator manufacturer to provide an efficiency map such as on the one in Figure 2.9 or an efficiency table, that the necessary data can be collected from. This efficiency data can be interpolated based on the given rotational speed and applied torque to determine the efficiency ratio at the given operating condition.

The power produced by the generator can then be calculated by Equation 2.16, for which that power is used to calculate the current produced using Equation 2.17.

$$Power_G = RPM \cdot Torque \cdot \eta_G \tag{2.16}$$

$$Current_G = \frac{Power_G}{Voltage} \tag{2.17}$$

Note that it is important for the voltages of the generator and battery to match the voltage of the electric motor. If the voltage supplied to the electric motor is lower than nominal, the electric motor will have decreased performance, or if the supplied voltage is too high there is a risk of overheating and damaging the electric motor.

2.5.4 Internal Combustion Engine

An internal combustion engine produces mechanical power through the combustion of fuel and is an option for the thermal machine part of the hybrid propulsion system. The amount of fuel is the limiting factor on how far and how long the aircraft can fly for, since the ICE is either producing power for the propeller or for charging the battery. The ICE model is defined by the following inputs and outputs in Table 2.4 in order to work with the simulation framework.

Table 2.4: ICE Model Inputs and Outputs

Input	RPM	Engine rotational speed
Input	$Altitude$	Aircraft altitude
Input	P	Air pressure
Input	$Temp$	Air temperature
Input	$Throttle$	Variable to control power
Output	$Power_{ICE}$	Engine power produced
Output	$Torque_{ICE}$	Engine torque produced
Output	$\dot{m}_F$	Fuel flow

This input and output structure is a general format meant to work with different types of internal combustion engines and different data sources. The details of the model will be specific to the chosen ICE and the type of data available. The $Throttle$ input controls the power setting of the ICE and can represent different physical variables depending on the given ICE data. If the given ICE data uses manifold pressure as an input, then manifold pressure can be the variable. Another common input for ICE data is the throttle setting expressed as a percentage, so that can also be used as the $Throttle$ variable.

The atmospheric pressure, P, is another important variable that can be used differently depending on the selected ICE. For naturally aspirated engines, the manifold pressure is limited by the atmospheric pressure, so the atmospheric pressure can be used to set a maximum manifold pressure available. Turbocharged engines can produce manifold pressures higher than atmospheric, though. Typically, a manifold pressure versus altitude curve is provided by the manufacturer, and this can be implemented into the ICE model with the given inputs.

The inputs to the ICE model are variables commonly used to look up engine performance in either tables or charts. Therefore, the ICE model can be constructed similarly to how the engine performance chart or table is read for the selected ICE. Either tabulated data can be inserted, or chart data can be digitized. Using the given inputs the data can be interpolated to find the outputs, and since the outputs depend on several inputs, a series of interpolations likely have to be performed.

2.5.5 Motor and Propeller Matching

In a propeller aircraft that is driven by an electric motor, the electric motor and the propeller would be physically connected by a drivetrain shaft. This forces the

motor and the propeller to rotate at the same speed, and when the power output of the motor is changed the resulting rotational speed of the motor-propeller system is the one that results in the motor and propeller having the same power and reaching equilibrium. In a simulation, there is no physical system that ensures the motor and propeller reach equilibrium, but it still needs to be implemented, so a motor and propeller matching model is required.

The motor and propeller matching model contains both the electric motor and propeller models within it, so the inputs are the same inputs required for both of those models from Tables 2.2 and 2.1. The outputs are also the same outputs from those models, but with an additional output of the rotational speed that results in the electric motor and propeller powers being matched.

It is an iterative process to find the rotational speed that matches the power of the electric motor and propeller. A general algorithm, shown in Algorithm 1, is to place the electric motor and propeller models in a while loop that iterates until the difference between the motor and propeller power is less than a specified error tolerance. The RPM_{in} input is the rotational speed of the electric motor and propeller from the previous timestep, and the RPM_{out} output is the rotational speed that matches the motor power and propeller power.

Algorithm 1: Electric Motor and Propeller Matching Algorithm

$RPM = RPM_{in}$;
while *error* $>$ *error tolerance* **do**
    $[Power_{EM}, Current_{EM}]$=**ElectricMotorModel**$(RPM, Torque)$;
    $[Thrust, Power_P]$=**PropellerModel**(RPM, V, ρ);
    $error = Power_{EM} - Power_P$;
    $RPM = RPM + 5 \cdot error$;
    $error = |error|$;
end
$RPM_{out} = RPM$;

This algorithm can be used with any electric motor and propeller combination as long as the electric motor and propeller models follow the inputs and outputs defined in Tables 2.2 and 2.1. The method for guessing the next RPM value in the while loop can be changed, but different methods are going to impact how computationally efficient and robust the algorithm is. Assuming the timestep of the simulator is sufficiently small, the aircraft state only changes slightly between each timestep, so it is beneficial to use an algorithm that looks for a solution that is close to the solution from the previous timestep. Therefore, setting the RPM_{in} to be rotational speed from the previous timestep and using it as an initial guess significantly decreases the number of iterations needed to converge.

In certain hybrid configurations such as a parallel or series-parallel hybrid, an ICE can drive the propeller as well. Thus, the power of the ICE and the propeller have to match, which is also the case for a conventional propeller aircraft. This uses the same iterative scheme as Algorithm 1 for finding the rotational speed that results in the powers being matched, only this time for an ICE and propeller. This can be achieved by modifying Algorithm 1 to use the ICE model instead of the electric motor model. Note that this model is only required if the ICE and propeller are directly connected. For certain hybrid configurations, such as a series hybrid, the ICE is connected to a generator. The next section discusses the requirements for pairing an ICE and generator together.

2.5.6 ICE and Generator Matching

The mechanical power produced by an ICE must be converted to electric power through a generator for some hybrid types. To do this, the ICE spins a shaft that is connected to the generator, so the power at both ends of the shaft must be the

same. There are two methods to ensure the power of the ICE and generator match depending on how the ICE is controlled.

For a hybrid aircraft, it can be desirable to set the ICE to operate at a certain condition in order to optimize performance parameters, such as minimizing fuel consumption. If this strategy is implemented, the user can set the rotational speed of the ICE to be a constant value. In this case, the specified ICE rotational speed input and the torque produced output from the ICE model must both be inputs to the generator model. Since power is the product of torque and rotational speed, forcing the ICE and generator to operate at the same torque and rotational speed ensures that the power at both ends of the shaft connecting them is matched. If the ICE is not constrained to operate at a specific rotational speed, then the process to match the powers is the same as Algorithm 1 but with the ICE and generator models contained instead.

2.5.7 Battery

The role of the battery, which is a system of electrochemical cells in series and parallel, is to store energy for the electric machine. The goal of the battery model is to have a high level of fidelity while also being easily configurable for different batteries available, which can be achieved by using the Simscape table-based battery model for Simulink [23]. This battery model uses data commonly found in battery and battery cell datasheets and also considers the charging and discharging dynamics of the battery. Importantly, the model reflects how the battery properties change with state of charge (SOC), which is the level of charge relative to the capacity, and temperature [24].

The data required for the battery model are the battery capacity, voltage, terminal resistance, and equivalent circuit parameters. A battery can be modelled as a Thevenin equivalent circuit with parallel resistor-capacitor sections, and the polarization resistances and time constants of these resistor-capacitor sections are needed to describe the dynamics of the battery [23, 25]. All of these parameters, which can be provided by the manufacturer or determined through testing, are tabulated for different SOC values and, if desired, temperature values. The initial SOC of the battery is also set in this model.

A battery is configurable in different manners, such as the cells that make up the battery, and then how many of those cells are in series and parallel. The necessary data for the battery model can be obtained from a battery datasheet of a battery that already exists, but it can be difficult to find a battery that fits the desired specifications. Therefore another option is to use cell data and modify it based on the desired number of cells in series and parallel. If using battery cell data, the voltage data for the battery model is the product of the cell voltage and number of cells in series, and the capacity data is the product of the cell capacity and the number of parallel cells. In this way it is simple to find battery cell data and then create a battery model with the desired voltage and capacity while still properly modelling the battery.

The input to the battery model is a current, with positive current charging the battery, and negative current discharging the battery. The output, and most important metric of the battery, is the SOC which represents how much energy is available from the battery. It must be tracked in order to control how the hybrid system delivers the power since if the SOC is too low, power cannot be drawn from the battery, and the battery must also stop charging once it reaches a high SOC. These minimum

and maximum SOC limits can be set in the energy management system, which is discussed in the next section.

2.6 Energy Management

Depending on the type of hybrid system modelled, there can be different ways to deliver the power required. To manage all of the potential paths of power flow, the energy management system uses a state machine, which based on an input action and current state, determines the next state of the hybrid propulsion system. Table 2.5 represents the minimum state machine, since in all hybrid configurations it is necessary to ensure that the battery gets charged when it reaches a minimum SOC and discharged when it reaches a maximum SOC. More inputs can be added, for instance vertical velocity increasing or decreasing, but this minimum state machine protects the battery from running out of charge in flight or over-charging.

Table 2.5: Hybrid System State Transition Table

Input	Current State	Next State
SOC crosses maximum	battery charging	battery discharging
SOC crosses maximum	battery discharging	battery discharging
SOC crosses minimum	battery charging	battery charging
SOC crosses minimum	battery discharging	battery charging

One requirement of the energy management system is to charge the battery when it reaches a low SOC, which according to Table 2.5 happens when the minimum SOC is crossed and the battery is charging. Note that there has to be output actions defined for each state transition in order to complete the change of state, but they will depend on the hybrid configuration. For instance, in a series hybrid, the ICE can be switched on to produce power for charging the battery when the battery SOC crosses the minimum and is currently in a discharging state. It is also important that

the output actions depend on both the input and current state. For example, if the ICE is simply toggled on and off when the minimum SOC is crossed without regard for the battery charging or discharging state, the ICE will turn on when the SOC falls below the minimum, and then turn off when the SOC rises above the minimum, resulting in the ICE being rapidly switched on and off and failing to fully charge the battery.

It is also required to ensure that the battery stops charging when it reaches a high enough SOC, which for the state machine happens when the maximum SOC is crossed and the battery is charging. If using the same series hybrid system as described before, the ICE can be switched off when the battery SOC crosses the maximum and the battery is in a charging state. This example would result in an on-off strategy of the hybrid system where the aircraft flies in electric only mode until the battery reaches the minimum SOC and then the ICE is switched on to charge the battery with excess power until the maximum SOC is reached and the ICE is switched off to begin electric only flight again. As mentioned, there are different strategies that can be implemented as long as the battery gets charged and discharged within certain limits.

2.7 Initialization

As discussed in Section 2.2, the state-space equations are integrated as an initial value problem, so the initial values of the state variables in Equation 2.4 must be specified. The first variable, which is the position in the horizontal direction, is always going to have an initial value of zero so that the variable can represent the distance flown. The horizontal velocity, vertical position, and vertical velocity can be determined from the speed and altitude profile that the user creates as the setpoints for the PID

controllers. By assuming the simulation begins with the aircraft in steady level flight, the initial value of the horizontal velocity is equal to the initial speed from the speed profile and the initial value of the vertical velocity is zero. The initial value of the vertical position is equal to the initial altitude from the altitude profile. The last state variable is weight, so the user must specify the initial weight of the aircraft.

Initial values for the control variables also need to be provided in order to start the simulation with the aircraft in steady level flight, which is a process known as trimming the aircraft. The lift coefficient required for steady level flight is the lift coefficient that results in the lift force being equal to the weight of the aircraft. This can be calculated by Equation 2.18 and is set to be the initial output of the lift coefficient PID controller.

$$C_L = \frac{2W}{\rho V^2 S} \tag{2.18}$$

In order to have constant velocity flight, the thrust force needs to be equal to the drag force. Using the initial lift coefficient from Equation 2.18, the initial drag coefficient can be determined from the drag polar in the aerodynamic properties model. The drag coefficient can then be converted to a drag force, which equals the steady level thrust force, by the following equation:

$$T = D = \frac{1}{2} C_D \rho V^2 S \tag{2.19}$$

To finish trimming the aircraft, it is necessary to find the value of the thrust control variable output by the thrust PID controller that results in the thrust equalling the drag force calculated in Equation 2.19. Essentially, this means finding the thrust control input to the hybrid propulsion system model that results in a specific thrust force. This can be done by running just the hybrid propulsion system model iteratively until the error between the thrust output and the steady level thrust force is small.

The resulting thrust control value is then set to be the initial output of the thrust control PID controller.

In determining the initial values, as well as being required inputs to various component models, the atmospheric properties need to be known. The simulator can use a standard atmosphere model, or any other, that defines the air temperature, pressure, and density as a function of altitude. The initial atmospheric properties can be calculated using the initial altitude, and during simulation the atmosphere model uses the altitude state variable to calculate the atmospheric properties at each timestep.

Chapter 3

VALIDATION

To validate the simulator, flight test data was gathered to use as simulator inputs and comparison to simulation results. The selected aircraft for testing the simulator was a Van's RV-7A, since there was access to an RV-7A that could provide flight test data. This RV-7A is equipped with a Dynon SkyView avionics system that logs data at a 16 Hz sample rate from aircraft sensors tied to the avionics system that give information such as speed, altitude, engine manifold pressure, fuel flow, and engine speed. A specific mission profile for a flight test was flown, and the altitude and true airspeed from that flight were used as speed and altitude setpoints for the simulator. In this way, it can be demonstrated that the simulator works as intended by following a given flight profile, and that the behavior of the simulated aircraft is representative of a real aircraft. Specific parts of the simulation framework, including the closed-loop control, ICE and propeller model methodology, and fuel consumption, can be validated through the results of this flight test.

3.1 RV-7A Model

To run simulations of the RV-7A, certain specifications and data are required to build the models. Models of the drag polar, propeller, and ICE were created using the methodology outlined in Chapter 2. The details of these models are specific to the RV-7A, and are not the only acceptable methods to create drag polar, propeller, and ICE models. The important factor is that the models follow the requirements

specified in Chapter 2 so that the components can seamlessly work together in the simulation framework.

3.1.1 RV-7A Specifications

The aircraft initial weight and wing reference area are the only aircraft specifications needed for the simulator. The wing reference area is used in converting the non-dimensional lift and drag coefficients to actual lift and drag forces acting on the aircraft. Other properties of the aircraft that define it's shape are not necessary because they are reflected in the drag polar.

Table 3.1: Van's RV-7A Specifications for Simulator

Weight	1,600 lbs
Wing Area	121 ft^2

3.1.2 Drag Polar

The drag polar must be in a format such that the coefficient of drag is only dependent on the coefficient of lift, so the drag polar of the RV-7A is expressed as an equation where the coefficient of drag is a function of the coefficient of lift, as defined by Equation 3.1 and plotted in Figure 3.1. This drag polar was determined through flight test data following the PIW-VIW method, which entails collecting data at different flight conditions [14]. The aircraft is first flown at maximum power until the airspeed has stabilized. Then the power is reduced in increments and the stabilized airspeed that results in level flight at each increment is recorded. The resulting drag polar curve from curve fitting the data is not parabolic, but it still only depends on the lift coefficient so it is an acceptable drag polar model for the simulation framework. The drag polar was also generated for steady flight, so it is considered a good approximation

since the expected simulations are not highly dynamic in terms of rapidly changing angles of attack.

$$C_D = .024292 + 1.66447 \times 10^{-9} C_L + .071696 C_L^2 \tag{3.1}$$

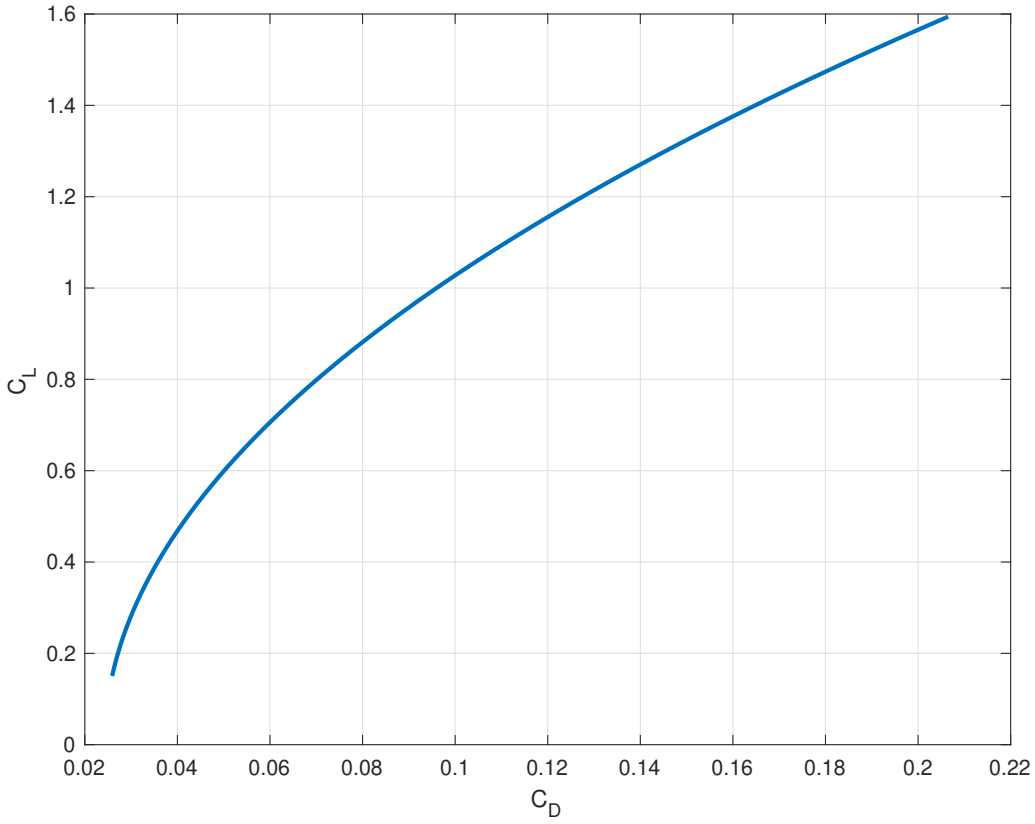

Figure 3.1: Drag Polar of RV-7A

3.1.3 Propeller

The required outputs of the propeller model are thrust and power, as previously discussed in the propeller model methodology, Section 2.5.1. The thrust and power are determined through finding the coefficient of thrust and coefficient of power, which are functions of advance ratio. Some propellers have data published by the manufacturer that include the coefficients of thrust and power at specified advance

ratios. If that's the case, that data can be interpolated at the actual advance ratio to find the coefficients of thrust and power, and then converted to actual thrust and power.

Such data for the propeller on the RV-7A was not available, so it was obtained using blade element momentum theory software. The propeller was 3D scanned to create geometry that was imported into the blade element theory software which provided data such as the coefficients of thrust and power across the range of advance ratios. Figure 3.2 shows the thrust coefficient and power coefficient of the propeller obtained from the blade element momentum theory software.

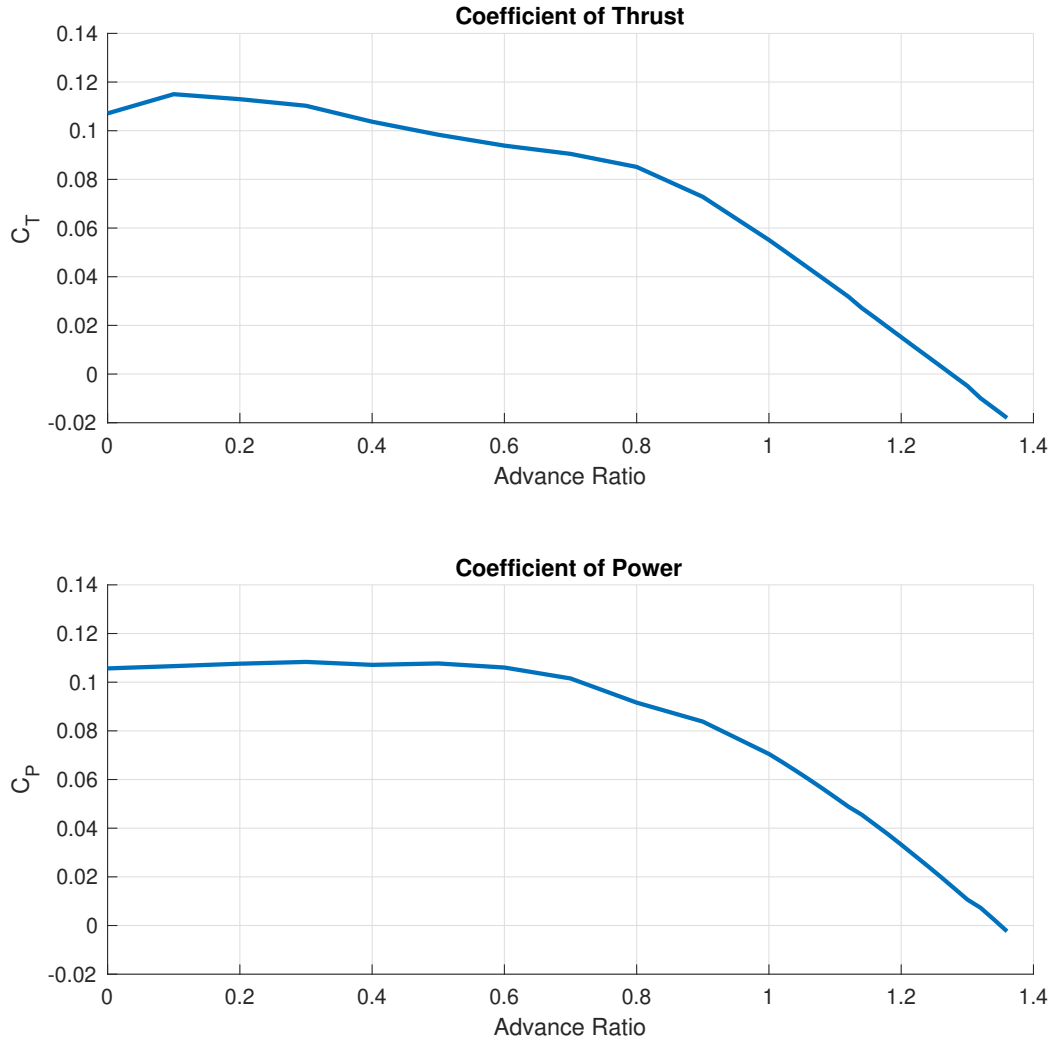

Figure 3.2: Propeller Coefficients of Thrust and Power by Advance Ratio

Given the propeller diameter, the advance ratio at each timestep is calculated using Equation 2.11. The coefficients of thrust and power are then interpolated from the data at the specified advance ratio, meaning they will lie on the curves in Figure 3.2. Lastly, the thrust force and actual propeller power are calculated using Equation 2.12 and Equation 2.13, respectively. This thrust force is an input to the state equations, and the propeller power is used in matching the ICE and propeller.

3.1.4 Internal Combustion Engine

The RV-7A is equipped with a Lycoming O360-A internal combustion engine, which is a 180 hp naturally aspirated engine. The Lycoming O360-A engine performance chart, included in Appendix A.1, was used as a data source to create an ICE model for the simulator. This engine performance chart provides the power and fuel flow given an engine speed, manifold pressure, altitude, and temperature which are also acceptable inputs and outputs for an ICE model based on the methodology in Section 2.5.4. Therefore, the model for this ICE follows similar steps to how the engine performance chart is read.

Since the engine data is not tabulated, the curves from the engine performance chart were digitized and entered as data in the ICE model. Through a series of interpolations based on the given manifold pressure, engine speed, and altitude, the standard temperature power is determined and then adjusted for temperature. The fuel flow is similarly calculated through a series of interpolations based on the manifold pressure and engine speed.

3.1.5 Engine and Propeller Matching

For the conventional RV-7A the propeller is connected to the ICE, so the power of the ICE and the propeller need to be matched according to the methodology in Section 2.5.5. Following that methodology, the ICE model and propeller models were placed within the ICE and propeller matching model which finds the rotational speed that matches the ICE power and propeller power. An example of how the matching function works can be seen in Figure 3.3, which shows the power curves for the ICE and propeller plotted for an altitude of 5,000 ft, manifold pressure of 20 inHg, true airspeed of 110 mph, and standard atmosphere conditions. The intersection point of these curves, represented by the black dot, is the rotational speed that the engine and propeller matching model solves for.

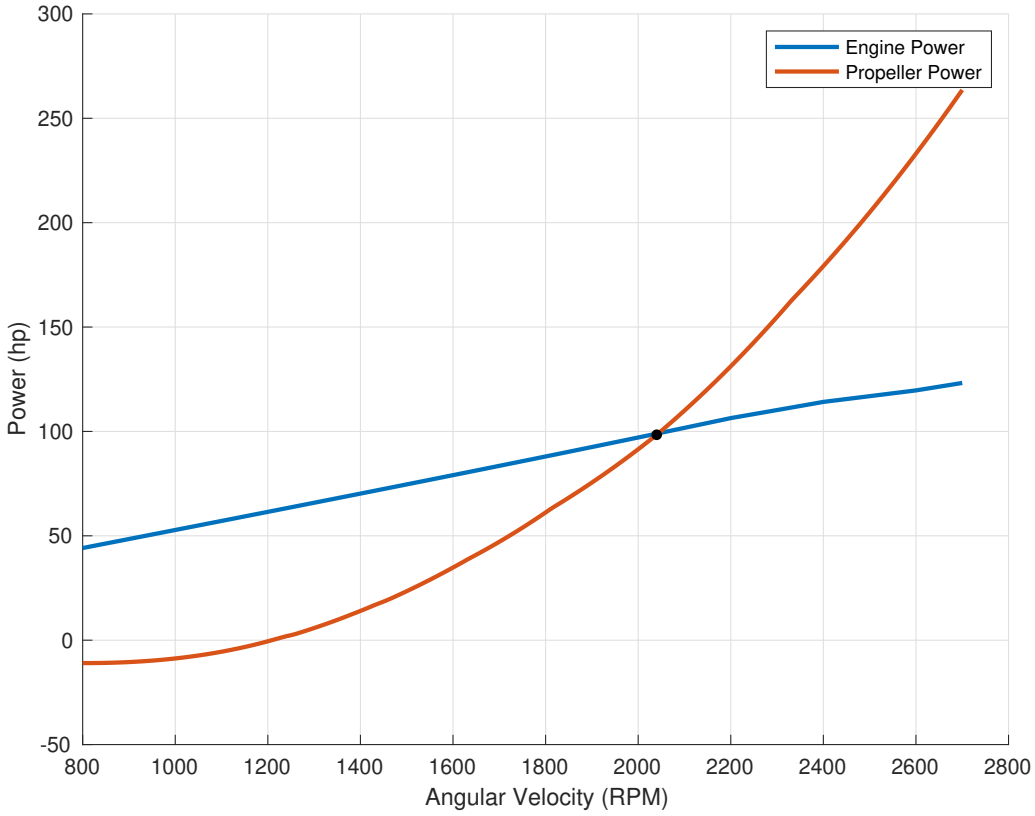

Figure 3.3: Internal Combustion Engine and Propeller Power

3.2 Mission Profile

The speed and altitude profile for this validation simulation is the measured true airspeed and altitude from the flight test data, which is plotted in Figure 3.4. Using the flight test data as the input for the simulator flight profile ensures that the simulated aircraft follows the same flight path that the real aircraft did during the flight test, which is important when comparing results. The mission profile for the flight test was designed to be the most complicated mission that the simulated aircraft would realistically follow. By proving that the simulator can follow the most complicated flight path, it is likely that the simulator can follow any other flight path given. The resulting mission profile was a series of six consecutive climbs and descents, with a different speed for the climb and descent segments so the aircraft will be required to simultaneously change altitude and airspeed. For each climb segment in the flight test, the throttle was opened to maximum continuous power, and for each descent segment, the throttle was closed to reach an engine speed just under 1,200 RPM. This engine speed results in a thrust coefficient of about zero, and if the engine speed was any slower, the propeller would create drag instead of thrust which is not advantageous to flight.

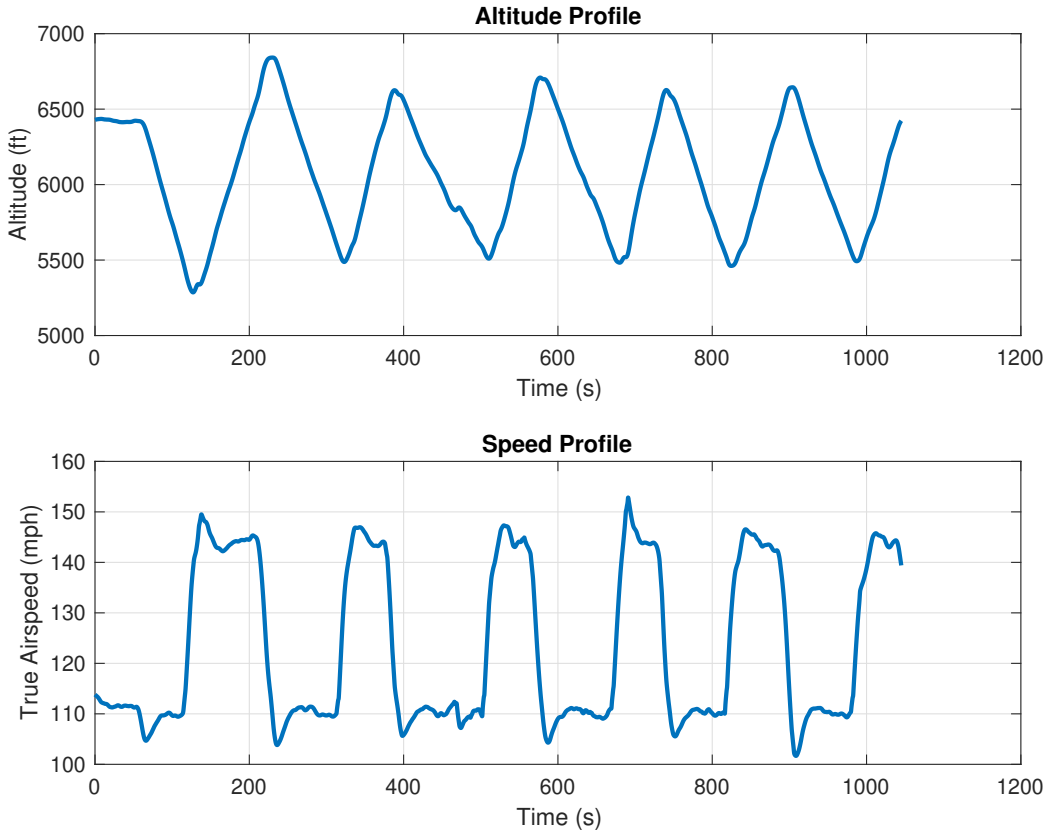

Figure 3.4: Flight Test Data Used for Simulation Inputs

3.3 Simulation Results and Validation

The true airspeed and altitude from the simulation are plotted along with the speed and altitude inputs in Figure 3.5. The results indicate the simulator can follow a given speed and velocity profile very well, and the significance of this is that the chosen control variables and PID control system successfully control the aircraft in the simulation. This simulated profile included simultaneous speed and altitude changes, so it is a complex profile to follow. Therefore, it is expected that the simulator can follow any flight path given as an input.

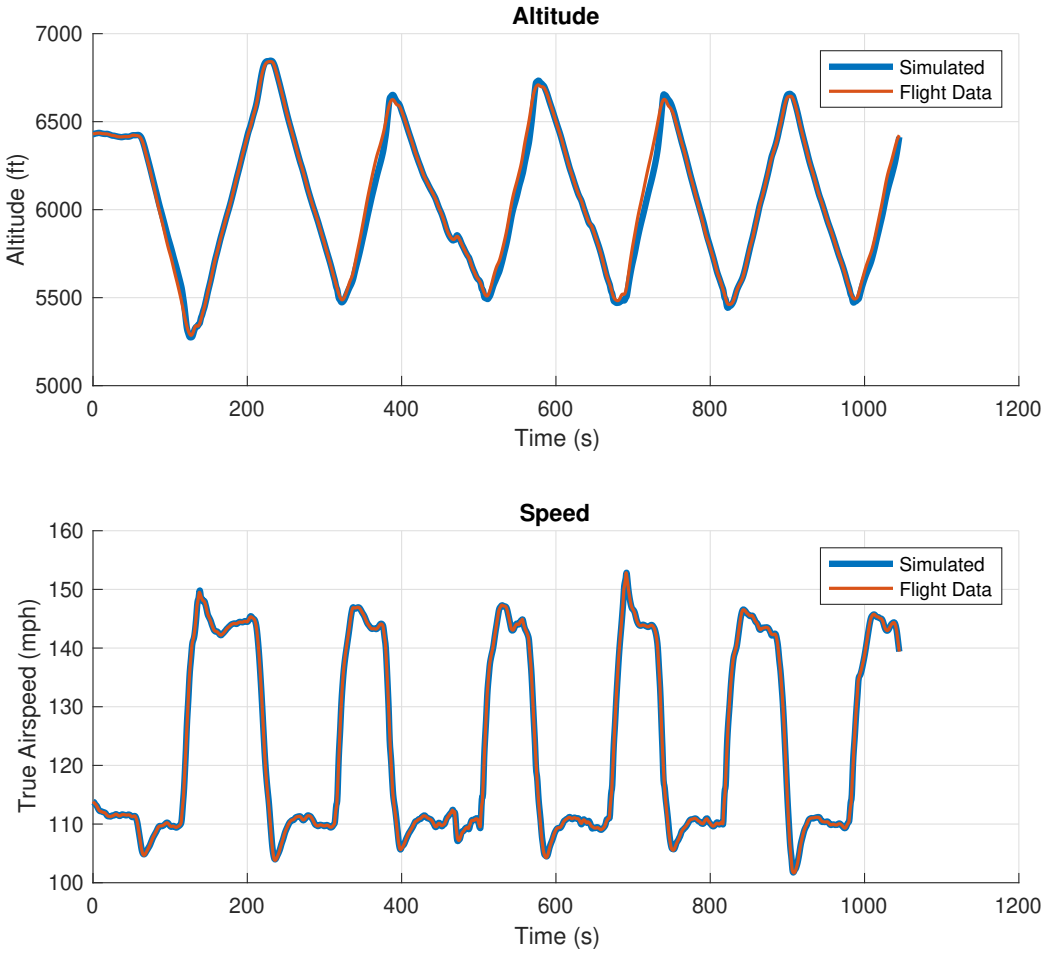

Figure 3.5: Altitude and Speed Results

To quantify the difference between the input profile and the simulated results, the percent error of the altitude and true airspeed are shown in Figure 3.6. The error is defined as the difference between the input profile and the simulated result, so a positive error is when the result is less than the desired input. While the aircraft is near steady state, when the rate of change of altitude and speed are low, the error remains extremely low. The error increases during more dynamic states when the rate of change of altitude and airspeed are higher, with a maximum altitude error of about 2.5% and maximum speed error of about 1%, but this error is still sufficiently low.

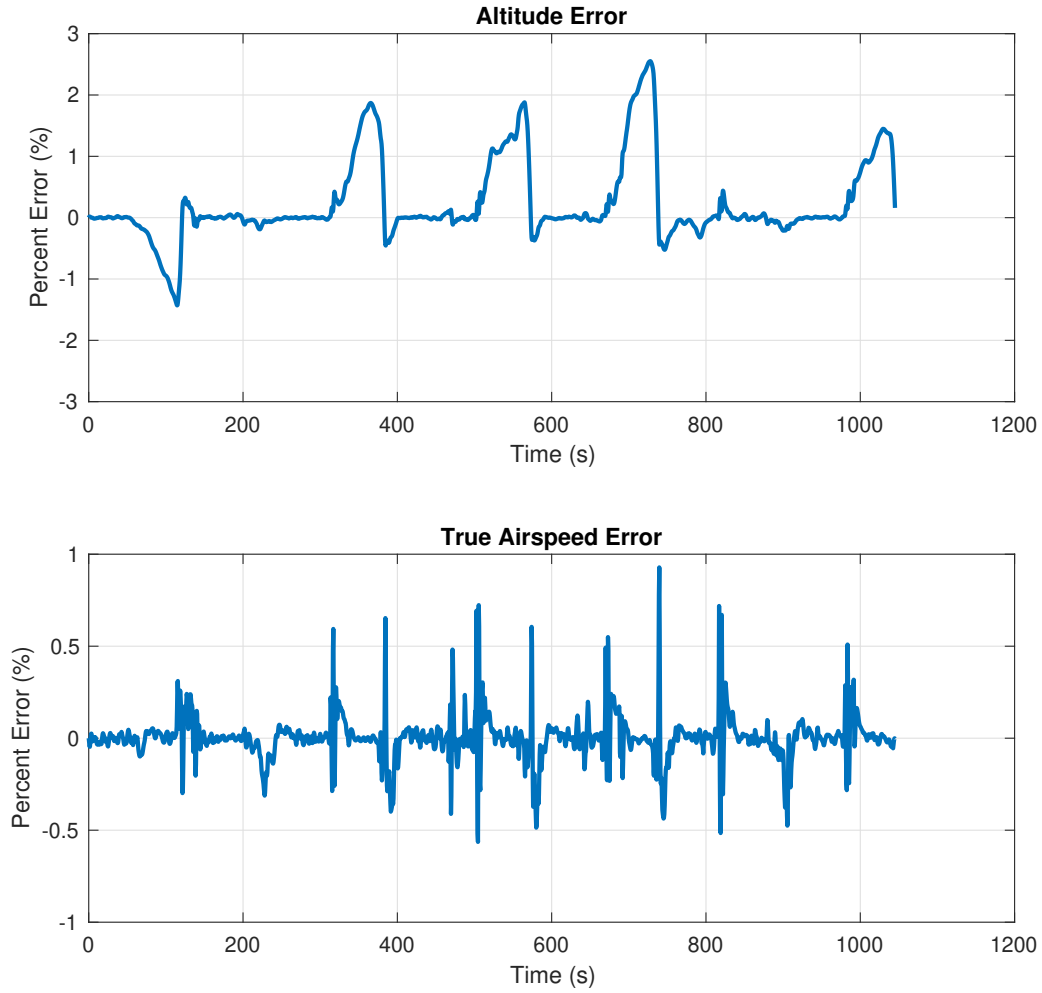

Figure 3.6: Altitude and Speed Errors

The altitude of the simulated aircraft is controlled by power, so for this simulation of a conventional aircraft, the thrust control variable output by the PID controller is the ICE manifold pressure. Increasing the manifold pressure increases the amount of power produced by the ICE by increasing the amount of air allowed into the combustion chamber. Figure 3.6 indicates that the altitude error increases when the input altitude profile changes from descending to climbing, which occurs because of the response time of the propulsion system. In reality, the power produced by an ICE and therefore thrust generated by the propeller cannot be changed instantaneously. Changes to a throttle lever are smooth, resulting in a smooth change in manifold

pressure and fuel flow for the ICE. This behavior is considered in the PID control of the manifold pressure so that there is realistic response time for the propulsion system. As a result, the altitude of the simulated aircraft can fall slightly behind the input altitude profile if the changes are too fast.

The airspeed of the simulated aircraft is controlled by the lift coefficient. In reality, the lift coefficient is changed by elevator deflection, and small changes in elevator deflection can occur at a relatively fast rate, so the response time of the airspeed control is faster than the altitude control. Figure 3.6 supports this behavior, as the airspeed error only briefly spikes when the airspeed profile changes.

The ICE manifold pressure is a control variable so it's behavior is important. Looking at the manifold pressure from the flight test and simulation in Figure 3.7, it is apparent that the manifold pressure output by the PID control in the simulation mimics the actual manifold pressure from the flight test. Therefore, the power is being adjusted in the simulation similar to how a pilot would adjust the power to fly the same mission. The ICE used in this case is naturally aspirated, so the maximum manifold pressure is the atmospheric pressure and during the maximum power climb segments the manifold pressure should decrease with the reduction of atmospheric pressure as the aircraft increases in altitude. This behavior can be seen in the flight data as well as the simulated manifold pressure in Figure 3.7.

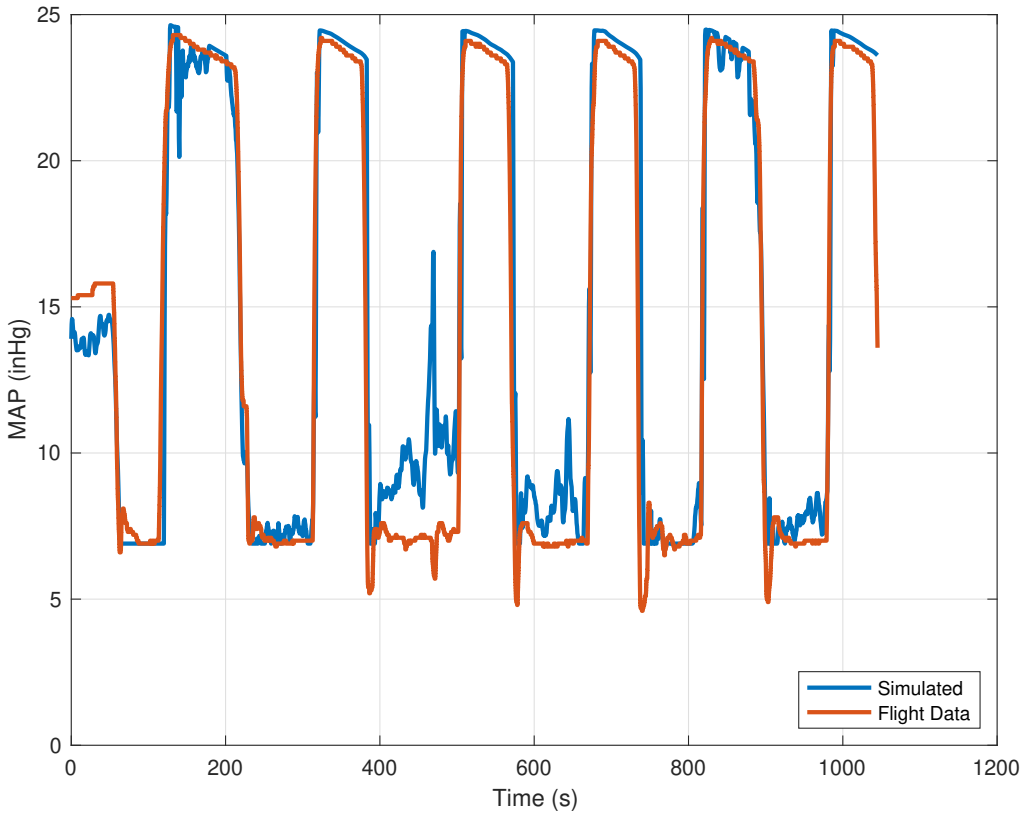

Figure 3.7: Combustion Engine Manifold Pressure Results

There are a few instances where the simulated manifold pressure deviates from the flight test data. This is due to using measured flight test altitude as the input. The deviation in manifold pressure such as the one occurring around 400-500 seconds into the simulation is from a bump in the altitude data, likely from an updraft in the flight test. When a user creates an altitude and velocity profile that is smooth, these jumps in certain simulated variables will not occur.

The engine speed from the flight data and simulated result are shown in Figure 3.8. Excluding the times when there are jumps in the input altitude profile, the engine speed from the flight data and simulation agree well. Engine speed is an important variable for a few reasons. The first is that it validates the ICE and propeller matching algorithm. The ICE power and propeller power need to be matched so that the power

on both ends of the shaft is the same, and this occurs at a certain rotational speed for the ICE and propeller. In a real flight, this will be forced by the physical properties of the propeller. The simulated engine speed, which is also the propeller rotation speed, agreeing with the flight data confirms that this matching of power is achieved at the correct rotational speeds.

The other reason the engine speed, and therefore propeller rotation speed, is significant is that the thrust produced by the propeller is dependent on the propeller speed. The thrust force is an input to state-space equations that govern the dynamics of the simulated aircraft, so it is important that the simulated thrust values are realistic. The thrust produced by the propeller cannot be directly measured in flight, though, so that is why the engine and propeller speed are being evaluated.

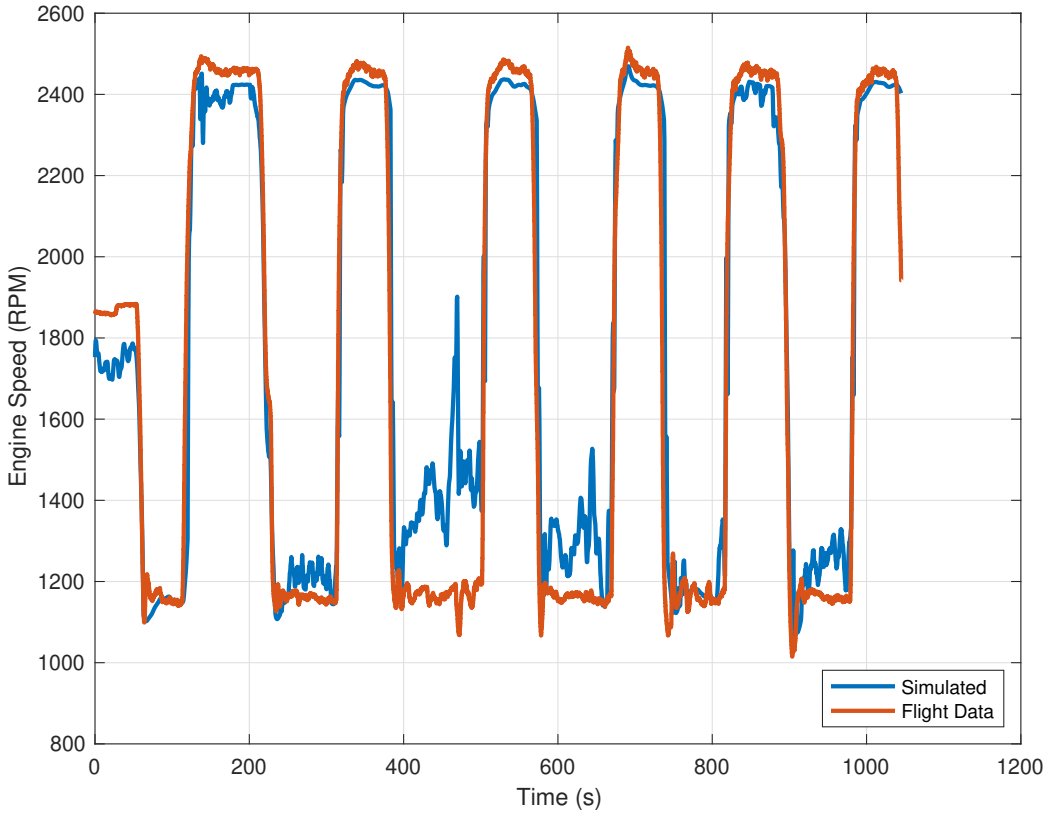

Figure 3.8: Combustion Engine Speed Results

The fuel flow rate and the amount of fuel consumed, which is the fuel flow integrated over time, are plotted in Figure 3.9. The most important part of the fuel consumption results are that the behavior of the fuel flow and fuel consumption are representative of a real ICE. One of the questions that the hybrid aircraft simulator can answer is how to minimize the fuel consumption, and for that, it is more important to look at the fuel consumption results comparatively, since if the ICE fuel flow model has some systematic error, it will not change what strategy is the most fuel efficient. Only the total fuel consumed would be less accurate, but it is not expected to have highly accurate fuel consumption results without further flight testing.

The primary source of error in the fuel flow model is due to the given fuel flow data. Fuel flow data on the engine performance chart is only shown for when the engine is producing above about 50% of rated power. So when the engine is operating at low power, such as during descent, the data is being extrapolated rather than interpolated which introduces error. Another source of error is due to the difference in the mixture ratio during the test flight compared to the mixture ratio used to collect the data for the engine performance chart. The exact mixture ratio is not specified for the performance chart data, and there is also no mixture sensor to log it during a flight test, so this can lead to fuel flow differences. For validation purposes, though, these results are still good since the fuel flow model is matching the given data, and the behavior of the fuel flow is representative of the real engine.

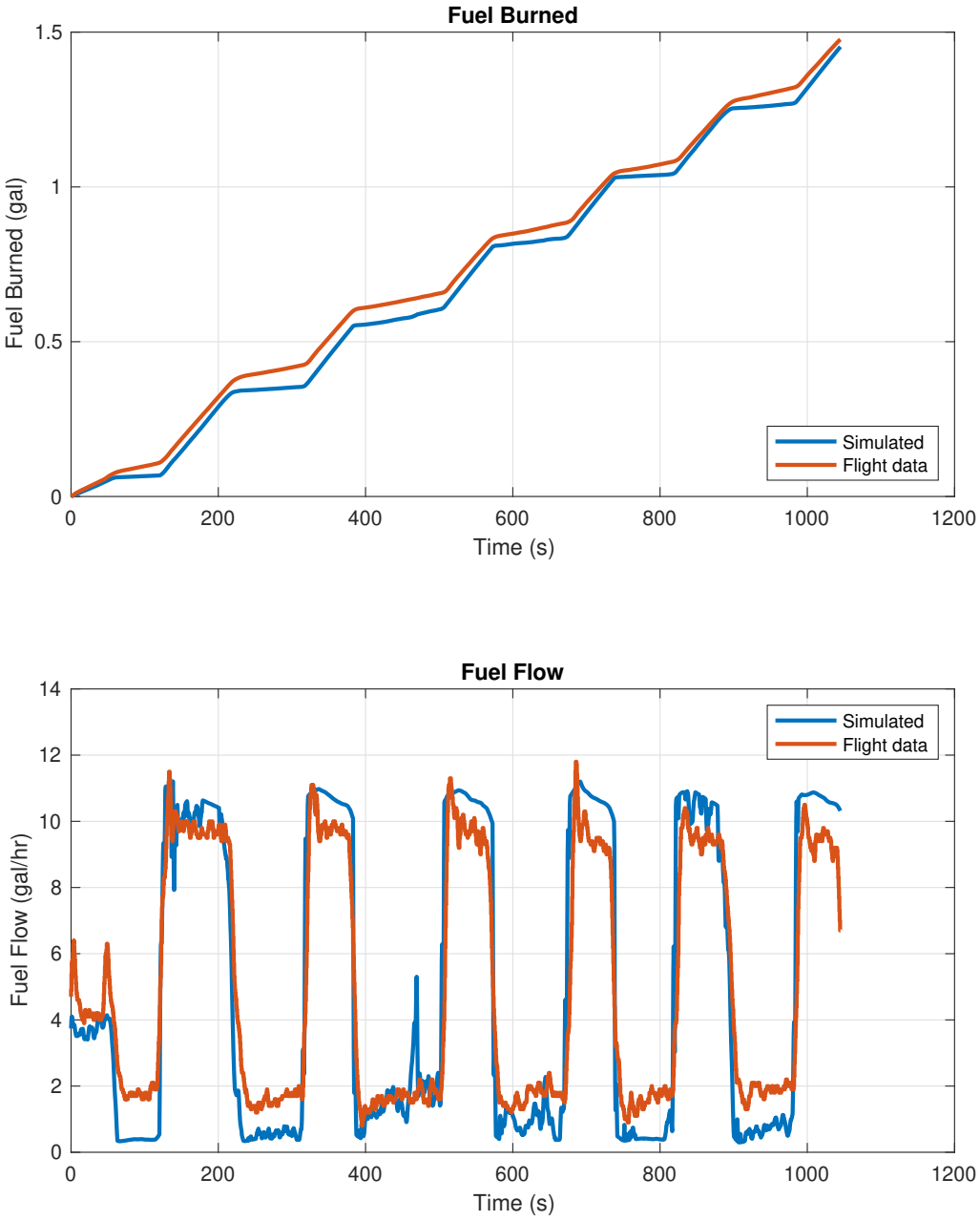

Figure 3.9: Combustion Engine Fuel Flow and Consumption Results

The results from the simulation agree well with actual flight test data of the aircraft, which validates crucial parts of the simulator. The simulator is able to, with high success, follow an altitude and airspeed mission profile input through the use of closed-loop control in the form of PID controllers that control the lift coefficient and thrust produced. The methodology for making models of the drag polar, ICE, and propeller

were also validated. Therefore, given that models for the hybrid propulsion system such as the battery, electric motor, and generator are valid, the simulator can produce accurate results for a hybrid aircraft. In the next chapter, the setup and results of a hybrid aircraft simulation are discussed.

Chapter 4

HYBRID AIRCRAFT SIMULATION RESULTS

This section will describe an example of modelling a hybrid aircraft and its propulsion system components in MATLAB Simulink, and provide results from simulating different flight path profiles. The purpose of this results chapter is not necessarily to analyze a specific hybrid aircraft, but rather to demonstrate the capabilities of the simulator and how it can be used as a design and optimization tool. Since this hybrid aircraft simulator can be used to model many different design configurations, a specific configuration must be chosen to obtain results.

4.1 Hybrid Aircraft Model

The hybrid aircraft modelled for obtaining results will be a factitious Van's RV-7A with a hybrid propulsion system, referred to as the RV-7H. For reference purposes, a standard Van's RV-7A will also be used, which was already modelled and simulated with successful results in Chapter 3. This reference RV-7A provides a working foundation for modelling a hybrid aircraft, and also serves as a reference for comparing the results of a conventional and hybrid aircraft. There is no hybrid aircraft flight test data available for validation of the full hybrid system, therefore the results will be focused on the comparison between the reference RV-7A and the hybrid RV-7H, along with comparisons between different flight profiles for the RV-7H.

For the simulation, the initial weight of the hybrid RV-7H will be kept equal to the initial weight of the standard RV-7A so that any differences in results are solely due to the hybrid propulsion system performance, and since the focus of the results is

to compare configurations rather than to obtain exact performance metrics. The aerodynamic properties, propeller, and ICE model are the same models used in the RV-7A validation simulation, so this section will discuss the electric motor, generator, and battery models that are added to assemble a hybrid propulsion system.

4.1.1 Electric Motor

The selected electric motor is an Emrax 268 axial flux motor and generator. This electric motor was selected because the maximum power output of 268 hp and maximum continuous power of 143 hp does not limit the performance when compared to the 180 hp internal combustion engine the standard RV-7A is equipped with [22]. An efficiency map provided by the manufacturer, shown in Figure 4.1, provided all of the necessary data for building the electric motor model according to the methodology in Section 2.5.2.

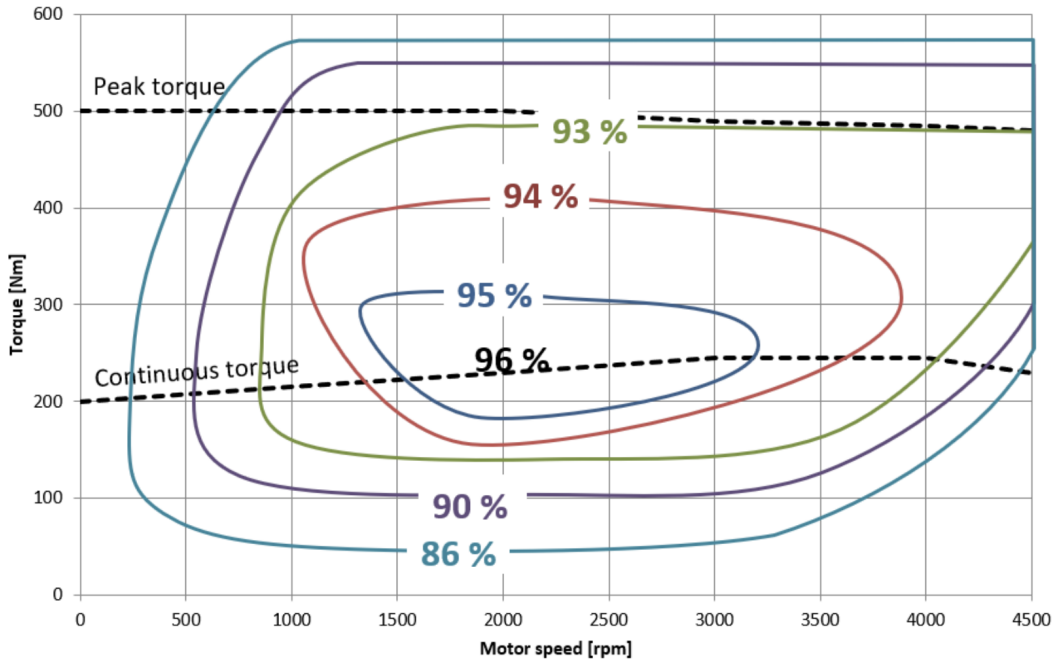

Figure 4.1: Efficiency Map of Emrax 268 Electric Motor [22]

For use in the model, the efficiency contours from Figure 4.1 were digitized and tabulated with the corresponding torque and motor rotational speed values, which are the two required inputs to the electric motor model. The model uses the given torque and rotational speed inputs to interpolate the efficiency ratio, which is used in Equation 2.15 to find the current required to produce the electric motor power calculated by Equation 2.14.

4.1.2 Generator

The Emrax 268 can also be used as a generator, and is adequately sized for the the 180 hp internal combustion engine that will power it. Using the Emrax 268 as both a motor and a generator also ensure that the voltages match. The same data from the efficiency map in Figure 4.1 can be used for the generator model, since the torque applied and the generator rotational speed are the required inputs to the generator model. Like the electric motor model, the generator model uses the given torque and rotational speed inputs to interpolate the efficiency ratio, though the equations that use the efficiency ratio are different. For the generator, the efficiency ratio is used to determine the power output by the generator, calculated by Equation 2.16, which determines the current that the generator produces found by Equation 2.17.

4.1.3 Battery

The battery is comprised of lithium-ion polymer cells, which have the specifications in Table 4.1. The battery cell data consists of no-load voltage, capacity, terminal resistance, polarization constants, and time constants at corresponding states of charge, which are the inputs to the Simscape table-based battery model described in Section 2.5.7. Data for a battery cell was chosen over data for a specific battery so that it

can be scaled to a desired configuration, since the voltage of the battery needs to be compatible with the electric motor. The electric motor has a maximum operating voltage of 250 volts, so the battery will consist of 60 cells placed in series to reach that voltage. This means that the no-load voltage data for the cell needs to be multiplied by 60 to use in the battery model. The cells have a capacity of 31 ampere-hours, which is sufficient for this application, so no parallel sections are needed.

Table 4.1: Kokam Li-ion Polymer Battery Cell Data [23, 26]

SOC (%)	**V0** (volts)	**AH** (A·hr)	**R0** (Ohm)	**R1** (Ohm)	**R2** (Ohm)	**R3** (Ohm)	τ**1** (s)	τ**2** (s)	τ**3** (s)
100	4.19	31	.0124	.0011	.0009	.0011	10.0	93.4	500
90	4.06	31	.0120	.0011	.0010	.0010	9.3	96.6	329
80	3.94	31	.0119	.0010	.0011	.0011	10.6	105.4	466
70	3.83	31	.0113	.0013	.0010	.0006	11.3	91.0	602
60	3.74	31	.0117	.0012	.0009	.0019	13.0	85.7	689
50	3.69	31	.0118	.0009	.0017	.0021	9.2	84.2	541
40	3.64	31	.0111	.0017	.0017	.0032	9.4	69.6	655
30	3.60	31	.0120	.0017	.0015	.0034	7.5	97.3	789
20	3.55	31	.0120	.0029	.0025	.0036	12.5	74.7	926
10	3.48	31	.0164	.0047	.0007	.0065	13.6	50.1	702

4.1.4 Hybrid Configuration

The components of the hybrid propulsion system will be arranged into a series hybrid, such as the series hybrid configuration in Figure 4.2. Since the propeller will be driven by the electric motor, the power of the electric motor and propeller need to be matched according to the methodology in Section 2.5.5, so the electric motor and propeller models are placed inside the model that finds the rotational speed that matches their powers. The power produced by the ICE is converted to electric power through the generator so it can either power the electric motor or charge the battery, so the power of the ICE and the generator also have to be matched. As described in the next section, the ICE will be operating at a specific rotational speed so by

following the methodology in Section 2.5.6, this same rotational speed must also be an input to the generator model along with the torque produced by the engine.

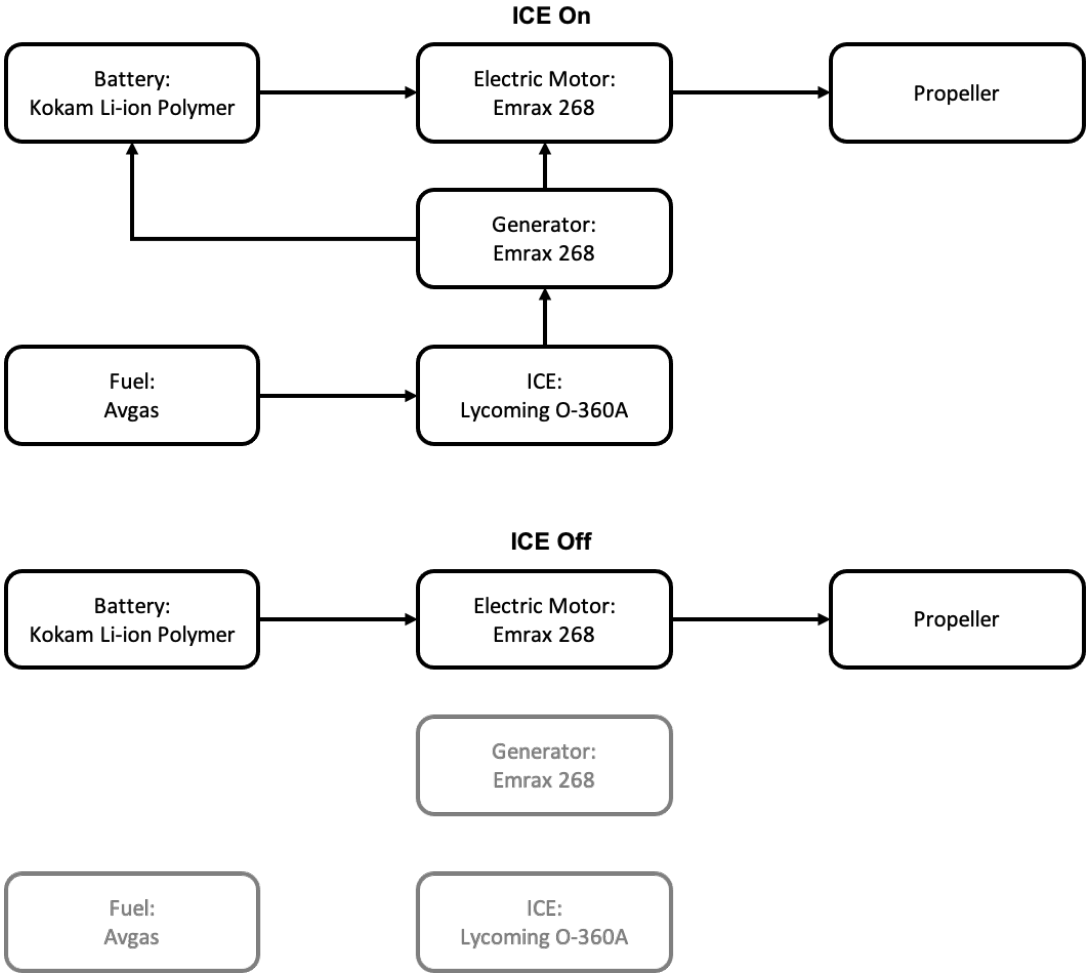

Figure 4.2: Series Hybrid Configuration of RV-7H

4.1.5 Energy Management Strategy

The hybrid propulsion system will operate in an on-off strategy where the ICE will be switched on and off. When the ICE is switched off, the aircraft will fly in electric only mode with all power coming from the battery, and when the ICE is switched on, it will charge the battery with the excess power available. It is desirable for the ICE to operate at a condition that attempts to minimize fuel consumption while also

providing enough power for flight and charging the battery, so this section will discuss how that operating point is chosen.

Looking at Figure 4.3, the power output of the ICE increases as the rotational speed and manifold pressure increase. It is desirable for the ICE to produce more power since it would result in a larger amount of excess power available to charge the batteries, but the fuel consumption, plotted in Figure 4.4, also increases with rotational speed and manifold pressure. In order to choose an operating point that balances the power output and fuel consumed, it is helpful to look at the brake-specific fuel consumption (BSFC), which is the power produced per amount of fuel burned. The BSFC of the ICE is shown in Figure 4.5, with a lower BSFC value meaning less fuel is consumed per amount of power produced, which is considered more efficient.

Another important efficiency metric to consider is the efficiency ratio of the generator, since the power produced by the ICE is sent to the generator. Looking at Figure 4.1, the region of high efficiency is at around 300 Nm of torque, or about 220 lb·ft, and moving away from this applied torque decreases efficiency. To help determine an operating point for the ICE, torque contour lines were included in Figure 4.5, with the line of 220 lb·ft constant torque being in the high efficiency region of the electric motor. Operating at a point that is close to this line and minimizes BSFC is considered an efficient operating condition for the ICE and generator pair to run at, so the operating point of the ICE will therefore be a rotational speed of 2700 RPM and a manifold pressure of 17.5 inHg, which is the point on the torque curve that minimizes the BSFC. Choosing a point below the 220 lb·ft torque curve would increase BSFC, but also reduce the power output and limit the charging rate of the batteries in addition to decreasing the efficiency ratio of the generator.

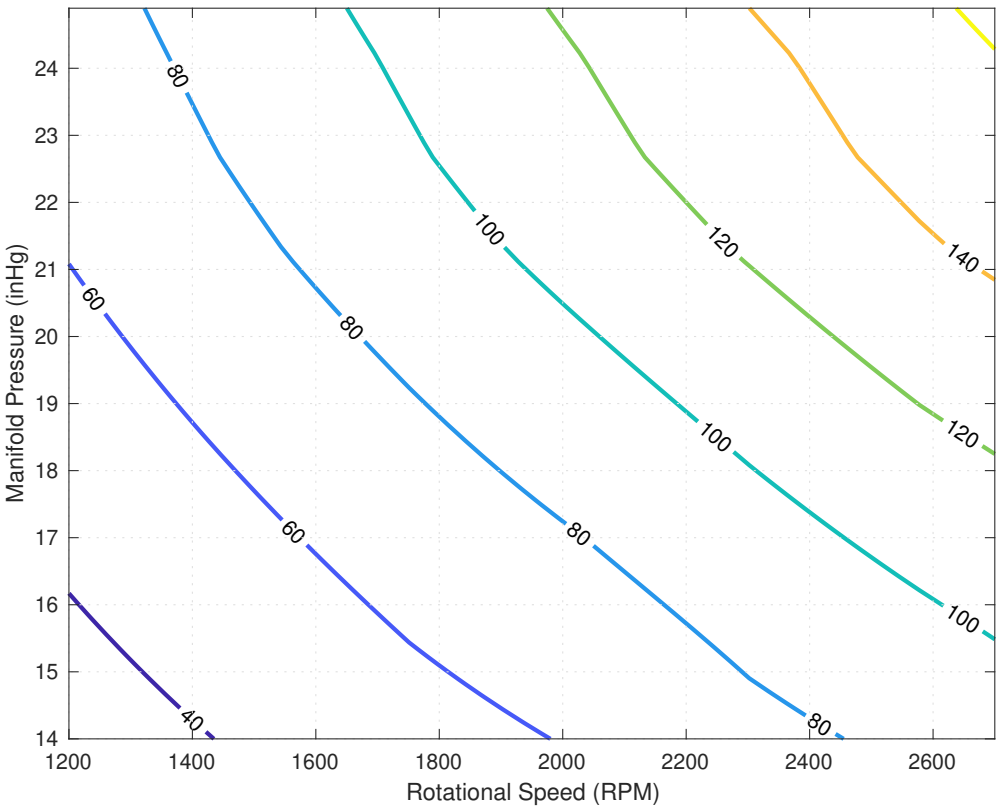

Figure 4.3: Power (hp) Contours of ICE

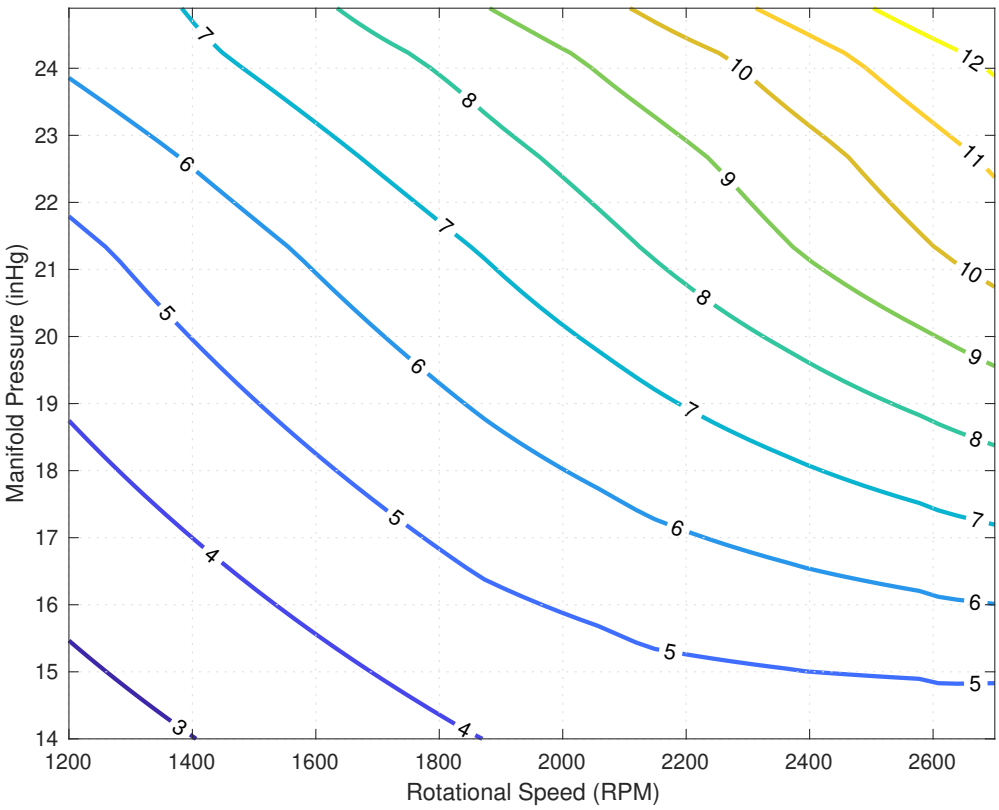

Figure 4.4: Fuel Flow (gal/hr) Contours of ICE

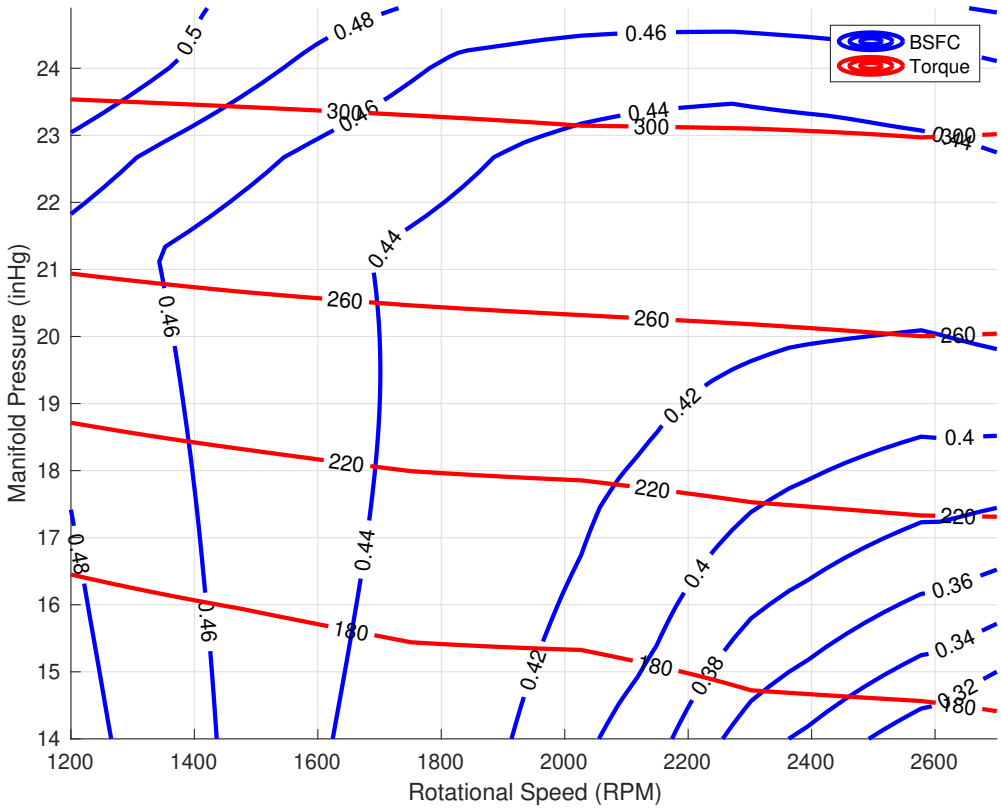

Figure 4.5: BSFC (lb/(hp·hr)) and Torque (lb·ft) Contours of ICE

Note that the torque produced by the ICE is the applied torque to the generator and the rotational speed of the ICE is the same rotational speed for the generator in order to ensure the power matches. It was already ensured that the torque value is in an efficient region of the generator by placing the torque curve on the BSFC map in Figure 4.5, but the rotational speed also needs to be considered. Referring to Figure 4.1, the rotational speed of 2700 RPM at 300 Nm of torque places the operating point of the generator in the region of peak efficiency, meaning the the operating point is efficient for both the ICE and the generator.

The other factor of managing the energy of the hybrid propulsion system is when to switch the ICE on and off, which is also when the battery is charging and discharging. The exact strategy will depend on the given flight path profile discussed in the

next section, but the limits for the minimum and maximum state of charge of the battery apply for any flight path to ensure the battery doesn't die or over-charge. The minimum SOC limit will be 20% so that a reserve amount of charge will be available for safety, and the maximum SOC limit will be 90% to protect the battery from over-charging. No matter what other strategies are implemented to control the on and off modes, these limits will be enforced by switching the ICE on when the SOC falls below 20% and switching the ICE off when the SOC reaches 90%.

4.2 Flight Path Profiles

The flight path profiles are designed to compare the fuel consumption of the hybrid aircraft, with the lowest fuel consumption translating to the highest range. It is known for a conventional propeller aircraft that maximum range occurs at the maximum lift-to-drag ratio speed and a constant altitude, but this may not be the case for a hybrid aircraft. To study how different ways of flying the hybrid RV-7H affect the fuel consumption, it will be simulated for various flight profiles and compared to the standard RV-7A.

The first flight profile, pictured in Figure 4.6, is the profile that would result in the maximum range for the standard RV-7A. The maximum lift-to-drag ratio speed is 100 mph, which is true for both the standard and hybrid aircraft due to having the same weight and drag polar, but again the maximum range speeds may not be the same. For this profile, the aircraft will fly 100 mph at a constant altitude of 5,000 feet, which is a typical altitude for singe engine propeller aircraft travelling around 75 to 100 miles. The hybrid RV-7H will fly in electric only mode until the battery reaches the minimum SOC of 20%, and then the ICE will be switched on until the battery reaches the maximum SOC of 90%.

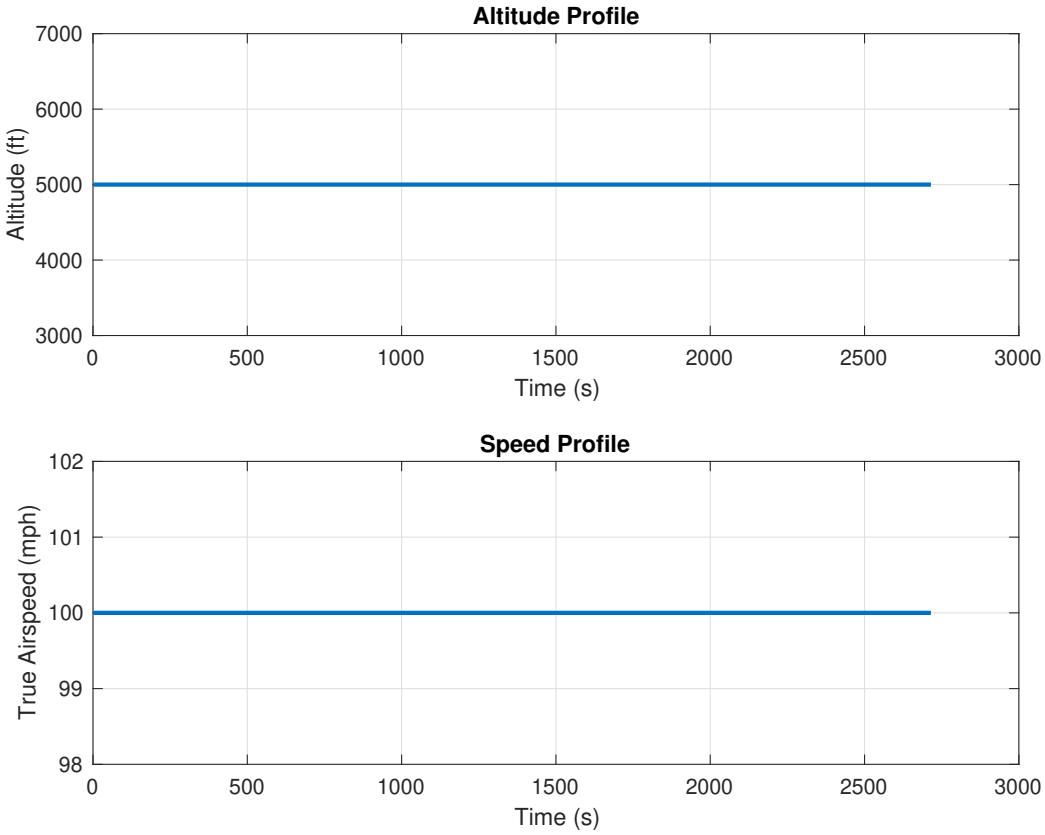

Figure 4.6: Level Flight Path Profile

The second profile, plotted in Figure 4.7, is to do cycles of climbing and descending at the maximum lift-to-drag ratio speed of 100 mph, with the climb and descend segments having a 2,000 ft change in altitude between 4,000 and 6,000 feet. For this profile, the strategy for operating the hybrid propulsion system is to climb with electric power only, and switch the ICE on during descent to charge the battery since there is more excess power available when descending.

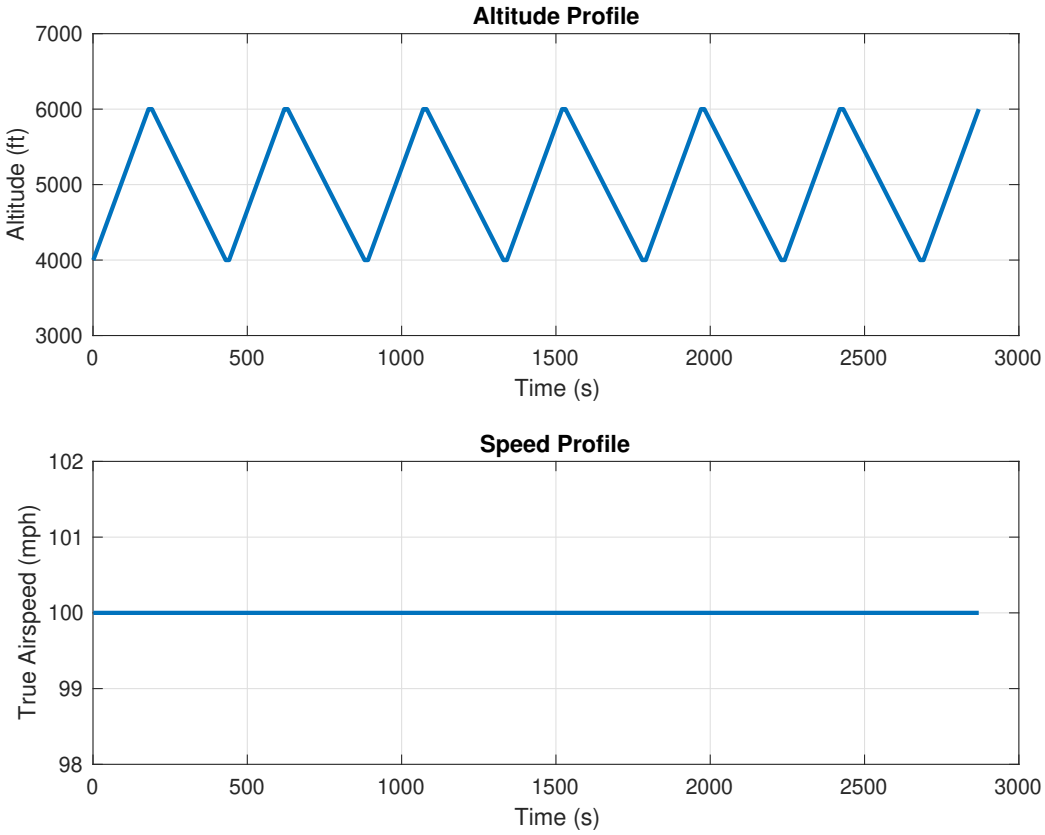

Figure 4.7: Climb and Descend Flight Path Profile

4.3 Simulation Results

The focus of the results is to demonstrate the capabilities of the hybrid aircraft simulator and to analyze the fuel consumption for different flight profiles in order to study the best strategy to fly the hybrid aircraft. As mentioned, the model of the hybrid RV-7H represents just one of many specific configurations for a hybrid aircraft, so the results are not meant to be conclusive for all hybrid aircraft but rather a demonstration of what kind of results the simulator can provide. First, results for the level flight profile will be presented, followed by the results of the climb and descent profile.

4.3.1 Level Flight

The fuel consumption for the RV-7A and RV-7H is plotted in Figure 4.8, with the hybrid RV-7H showing considerable fuel savings. Over the 75 mile flight, the standard RV-7A consumed 2.708 gallons of fuel, whereas the hybrid RV-7H consumed only 1.808 gallons of fuel, which is a fuel savings of about 33%. Note that this is an ideal fuel savings since the weight of the factitious hybrid RV-7H is the same as the RV-7A, but the plotted fuel consumption indicates that the ICE is being switched on and off. The fuel consumption of the standard RV-7A at this constant altitude flight at 100 mph is important because it is the maximum range condition, and therefore consumes the least amount of fuel per distance travelled, so it serves as a reference point for all other results in terms of efficiency.

An interesting trend to note from Figure 4.8 is that when the ICE is running for the hybrid RV-7H, the rate of fuel consumed, or the fuel flow rate, is higher compared to the RV-7A. However, since the ICE is switched off and on for the hybrid, it consumes less fuel over the whole flight. Another factor that leads to fuel savings for the hybrid RV-7H is that the ICE is operating at a lower BSFC compared to the standard RV-7A. As described in Section 4.1.5, the operating condition for the ICE in the hybrid configuration is 2700 RPM and 17.5 inHg manifold pressure, which has a BSFC of 0.38 lb/(hp·hr) from Figure 4.5. The engine speed and manifold pressure needed for the conventional aircraft to fly this flight profile was about 1600 RPM and 14 inHg, respectively, which results in a BSFC of about 0.45 lb/(hp·hr) according to Figure 4.5. This higher BSFC for the conventional RV-7A means that less power was produced per amount of fuel consumed compared to the hybrid.

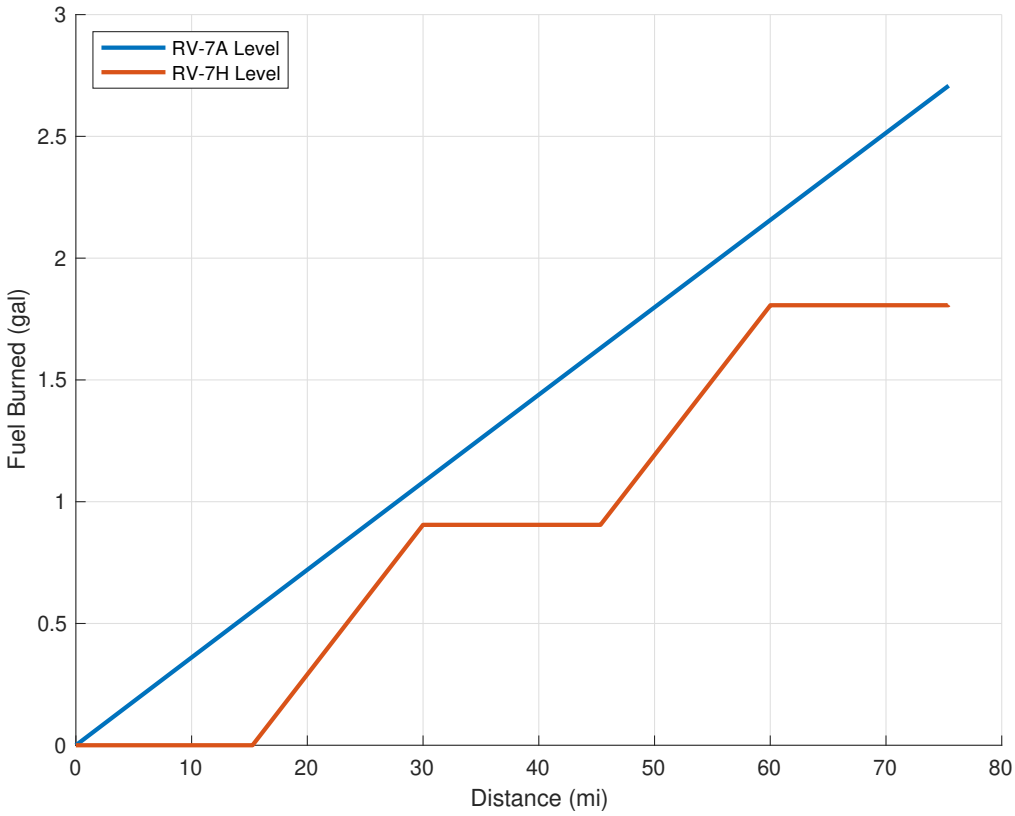

Figure 4.8: Fuel Burned for Level Flight Profiles

The performance of the hybrid propulsion system throughout the flight is plotted in Figure 4.9. It is evident that the hybrid system is operating as intended since the SOC of the battery charges and discharges when it reaches the minimum limit of 20% and maximum limit of 90%. The figure also shows how the hybrid propulsion system delivers the power required to sustain the flight path, which is constant for this steady speed and altitude flight profile. While the aircraft operates in electric only mode all of the required power is supplied by the battery, and then when the ICE is switched on the generator begins supplying power. The dashed green line, which is the power from the battery, is negative when the battery is being charged because it is taking away from the available power that the generator is producing.

The difference between the power from the generator and the required power represents the excess power from the generator, which is the amount of power available to charge the battery, and is also plotted in Figure 4.9. A higher amount of excess power translates to a faster charging time for the battery, which can be done by increasing the power produced by the ICE but will increase the fuel flow rate and decrease the BSFC. Another way excess power can be increased though is by decreasing the power required for flight, which can be done by trading potential energy in the form of altitude for kinetic energy to sustain speed. This strategy of charging the battery while descending is studied in the next set of results.

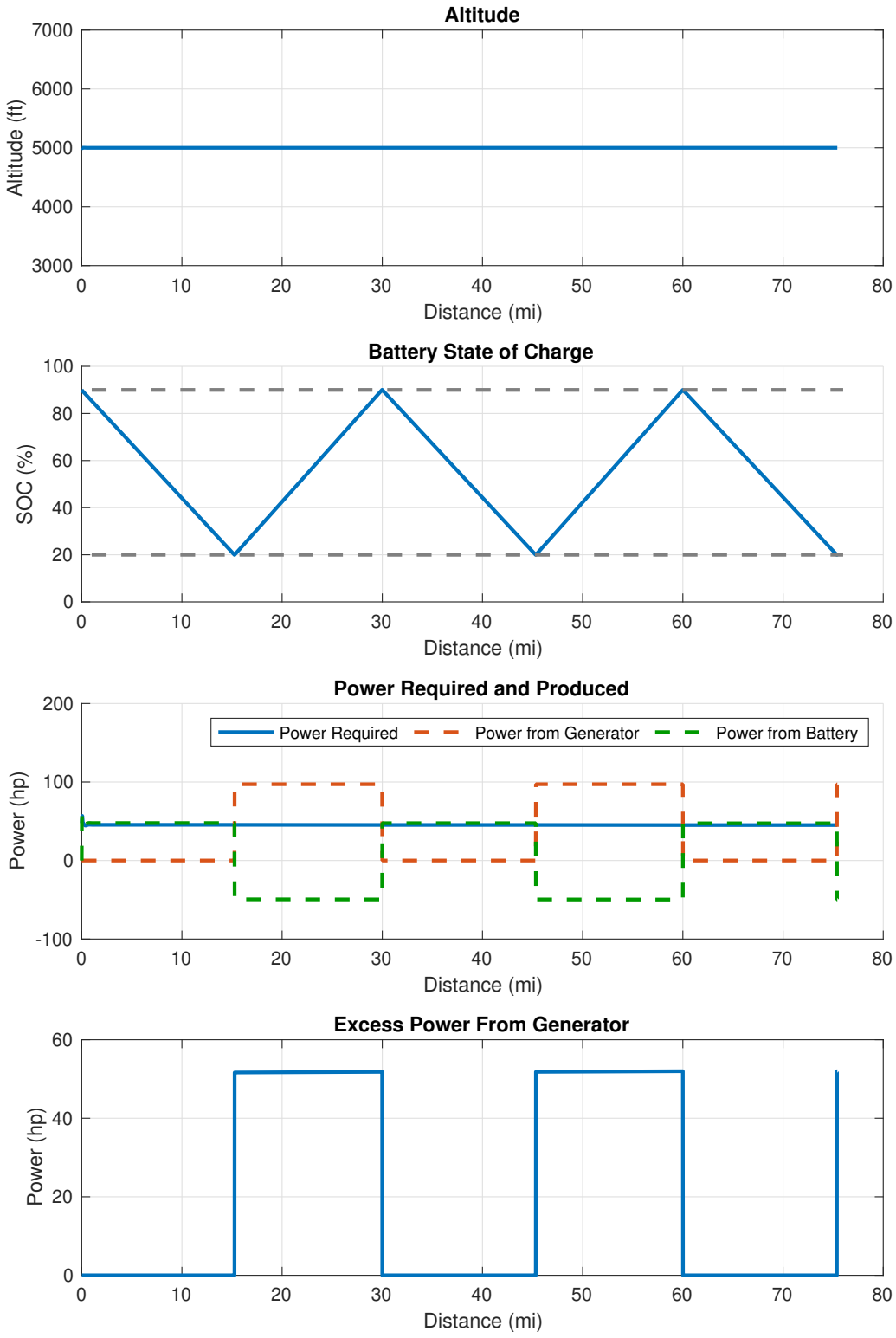

Figure 4.9: Hybrid Level Results

4.3.2 Climb and Descend Cycles

For the climb and descend flight profile, the hybrid RV-7H climbs with electric power and then descends with the ICE on to charge the battery. The fuel consumption of both the standard RV-7A and hybrid RV-7H is graphed in Figure 4.10, along with the fuel consumption of the previous steady level profile for comparison. As expected, the fuel consumption for the standard RV-7A increases when compared to level flight, but the fuel consumption of the hybrid RV-7H also increases for the climb and descend profile compared to level flight. Over the 80 mile climb and descend profile, the hybrid aircraft consumed 2.614 gallons of fuel compared to 3.352 gallons of fuel for the standard RV-7A, which is a 22% savings in fuel for the hybrid. It is clear, though, that for this speed of 100 mph, it is more efficient to fly the conventional or hybrid aircraft at a constant altitude compared to climbing and descending. Note that for simulations of the hybrid aircraft, the flight profile is designed to end when the SOC of the battery is low, since landing with a charged battery would not be an efficient use of power generated from the ICE. This is observed in Figure 4.10 by the segment of no fuel consumption at the end of the simulation.

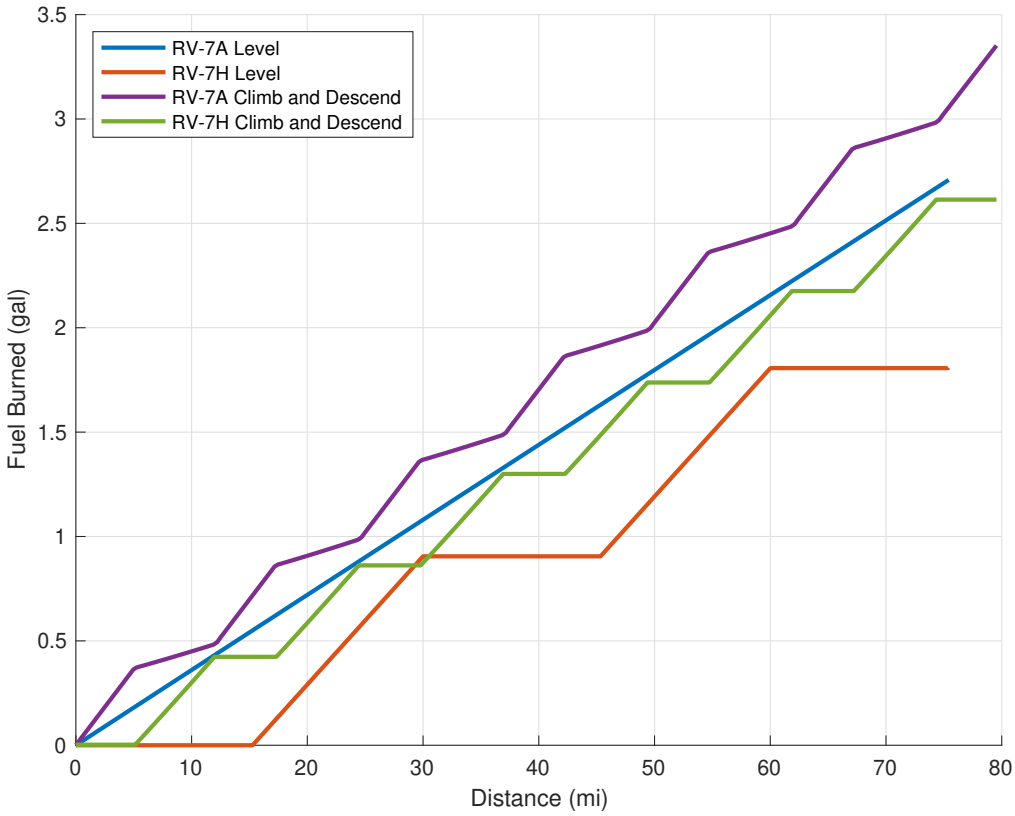

Figure 4.10: Fuel Burned for All Flight Profiles

The performance of the hybrid propulsion system for the climb and descend profile is pictured in Figure 4.11. For this profile, the ICE is off during climb and the battery discharges, and during descent the ICE is switched on to charge the battery. While this strategy is different than the level profile where the battery got charged and discharged to the minimum and maximum limits, the battery SOC still stays within the minimum and maximum limits for the climb and descend profile. The power required during climb is greater than the power required for the level profile so the battery discharges at a faster rate, but the power required during descent is lower. This means that the amount of excess power available to charge the battery is greater and the battery charges faster. Comparing the battery SOC plot of the level profile in Figure 4.9 to the climb and descend profile in Figure 4.11, there are more charge

and discharge cycles for the climb and descent profile due to this difference in power required.

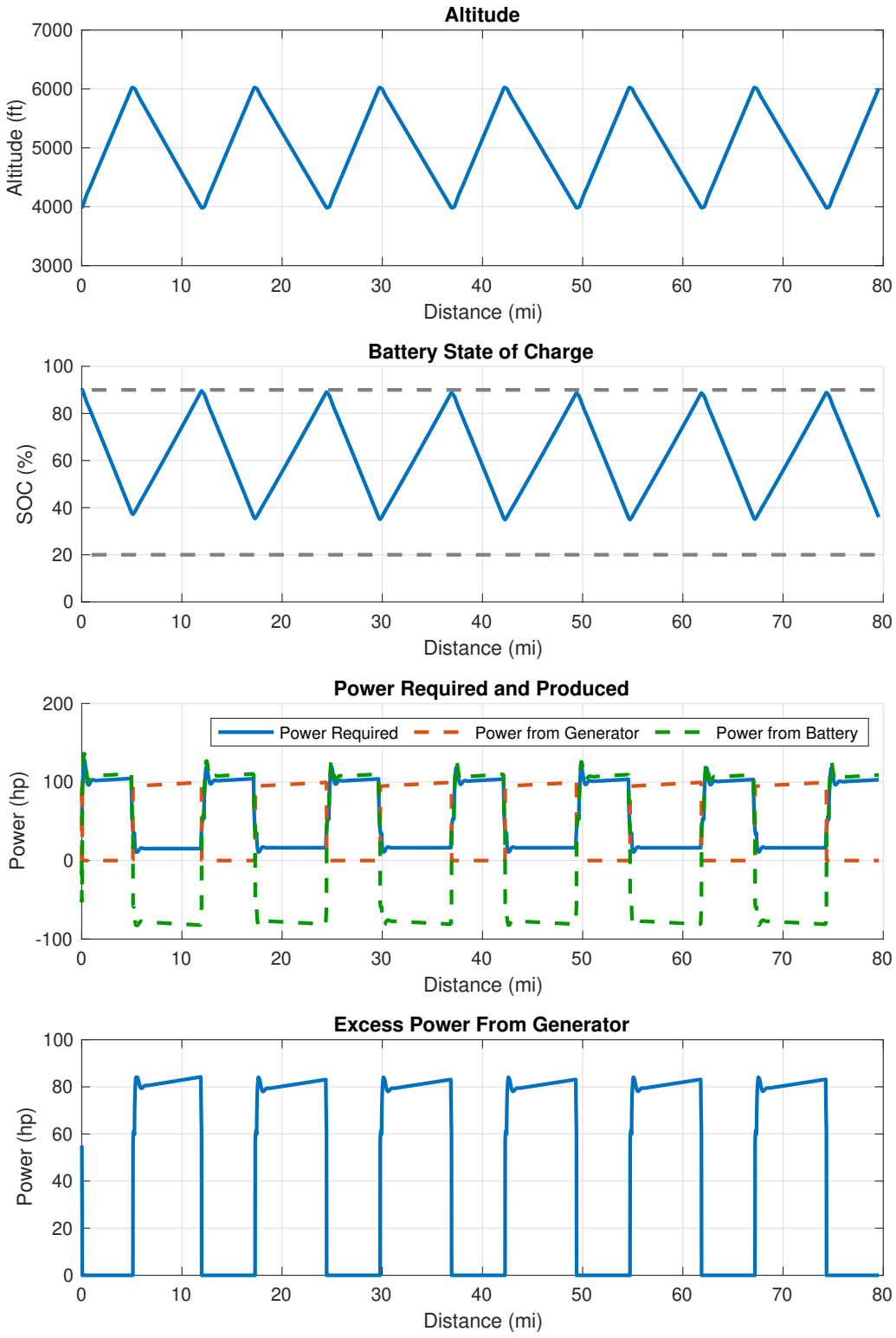

Figure 4.11: Hybrid Climb and Descend Results

4.3.3 Potential Optimization

The results from Figure 4.10 showed that level flight was more efficient than climbing and descending, but that is for flying at the maximum lift-to-drag ratio speed of 100 mph. It is worth investigating if this trend holds true for other flight conditions, so another set of level flight and climb and descend profiles was simulated at 125 mph. These results also demonstrate how the simulator can be used as an optimization tool to find how to best fly and operate the hybrid aircraft for minimizing fuel consumption.

The level flight profile illustrated in Figure 4.12 is for 5,000 at 125 mph, and the climb and descend profile in Figure 4.13 is also at 125 mph. Since there is less excess power available while descending at 125 mph compared to 100 mph, the duration of each descent segment is longer in time for 125 mph so that the battery can still be charged.

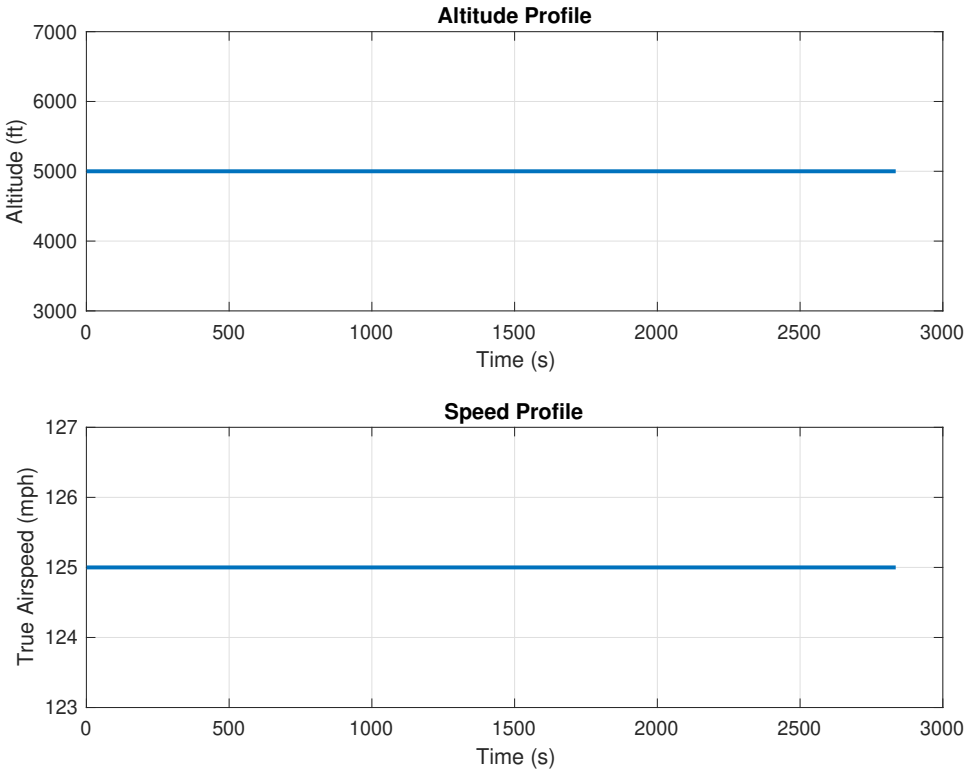

Figure 4.12: Level Flight Path Profile at Faster Speed

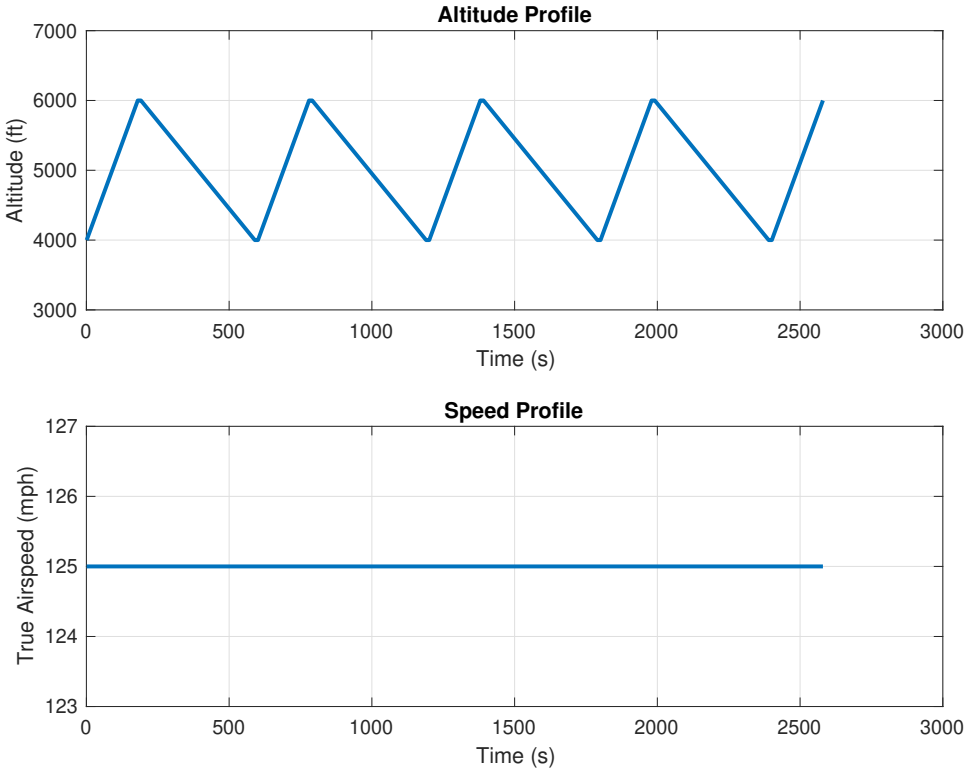

Figure 4.13: Climb and Descend Flight Path Profile at Faster Speed

The fuel consumption of the level flight and climb and descend profiles at 125 mph are plotted in Figure 4.14, in addition to the results from 100 mph, for the hybrid RV-7H. These results are significant because at 125 mph the difference in fuel consumption between the level flight and climb and descend profile appears to be much smaller compared to at 100 mph. This suggests that at certain speeds it could be possible that flying level is less efficient than climbing and descending. At a high enough speed, though, the excess power available will be too small to charge the battery in a reasonable amount of time, or at all, so this becomes an optimization problem that the simulator can potentially be used for.

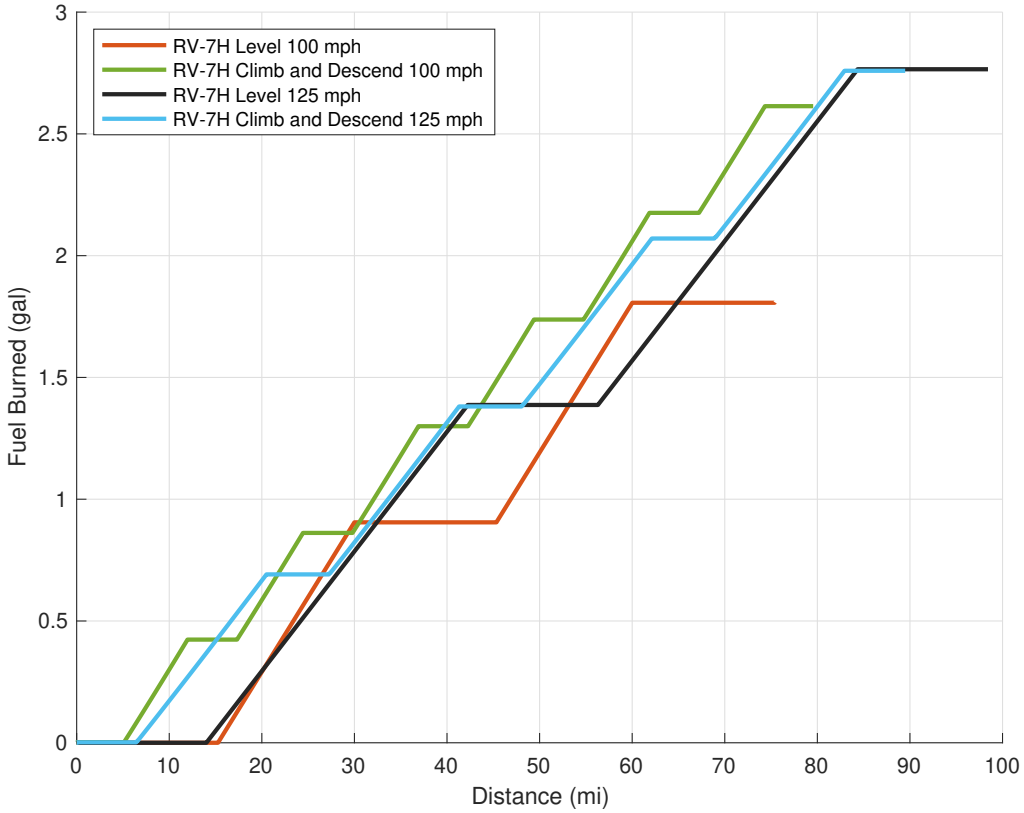

Figure 4.14: Fuel Burned at Different Speeds

The amount of fuel consumed for the level flight at 125 mph was 2.765 gallons over 98 miles, and for the climb and descend profile it was 2.759 gallons over 89 miles. Since each flight profile ended after a climb segment so the battery power was utilized, the

number of miles flown for each flight profile varied and thus the total fuel consumed cannot be directly compared to determine which profile was the most efficient. So, the next section will analyze the fuel consumption in a proper method.

4.3.4 Analysis of Fuel Consumption

Comparing the total fuel consumed is only valid for comparing the conventional versus hybrid aircraft for the same mission profile since the distance flown was the same. For comparing the fuel consumption from different mission profiles, it is useful to evaluate fuel consumption as fuel consumed per unit distance, for which the lowest fuel consumed per distance translates to the best range. Table 4.2 summarizes the fuel consumption for each simulated profile in gallons per 100 miles from most efficient to least efficient so that the different profiles can be validly compared.

Table 4.2: Fuel Consumption for Simulated Flight Profiles

Altitude	Speed (mph)	Configuration	Fuel Consumption (gal/100mi)
Level	100	RV-7H	2.397
Level	125	RV-7H	2.809
Climb and Descend	125	RV-7H	3.083
Climb and Descend	100	RV-7H	3.286
Level	100	RV-7A	3.591
Climb and Descend	100	RV-7A	4.214

The most efficient flight path profile for the hybrid RV-7H that was simulated was for level flight at 100 mph, which suggests that the maximum range condition for the hybrid RV-7H is the same maximum range condition for the standard RV-7A. At 100 mph, the level flight profile uses 27% less fuel than the climb at descend profile for the hybrid configuration, but at 125 mph the level flight profile is only 9% more efficient. This trend means that it could be more efficient to fly a climb and descend

profile at a certain speed. However, at 150 mph, the amount of excess power reduces enough that it takes an unreasonable amount of time to charge the battery.

In summary, the minimum fuel consumption and therefore maximum range condition for this hybrid aircraft is level flight at 100 mph, but if it is desired to fly at other speeds it could be possible that a climb and descend profile is more efficient. To find the solution to that hypothesis, though, a more complete optimization of flight path profiles would have to be conducted. For the scope of this project, these results demonstrate that the simulator can be used to compare the performance of the hybrid propulsion system for different flight path profiles. Keep in mind that these results are only one potential way that the simulator can be used as a tool for designing and optimizing a hybrid aircraft. For instance, the simulator could be used to similarly compare the performance of the hybrid propulsion system using different battery models for the same flight profile.

Chapter 5

CONCLUSION

5.1 Summary

A configurable hybrid aircraft simulator was successfully assembled and capable of simulating the performance of a hybrid propulsion system over a given flight profile with considerably small tracking error. The requirements for each hybrid system component model and aircraft model subsystem were defined in order to ensure the simulation framework remains functional for any configuration of hybrid architectures. Simulation results were also compared to flight test data to demonstrate that the behavior of the simulated aircraft is representative of a real aircraft, and to validate the PID control strategy that controls the aircraft's speed and altitude. A design for an aircraft with a series hybrid propulsion system was modelled and simulated over different flight paths to evaluate the performance of the hybrid system. Importantly, the results demonstrated how the simulator can capture the effects that the hybrid system design and flight strategy has on important metrics of hybrid aircraft performance, and therefore prove the use of the simulator as a design and optimization tool for specific goals.

5.2 Future Work

Future work can be split into work that can be done on the simulator and then work that can be performed using the simulator as a tool. The highest priority task for improving the simulator would be to successfully implement a hydrogen fuel cell model.

Due to the lack in fuel cell data available and unsuccessful attempts to purchase a fuel cell for testing, a model of a hydrogen fuel cell was not implemented. Another feature that could be useful would be to create a database of hybrid propulsion system component models, and a user interface or initialization script that allows the user to select components.

The simulator built for this thesis does not consider winds, but could easily be added by modifying how the true airspeed is calculated in the aircraft dynamics model and accounting for winds. The simulator is also a point mass model with two degrees of freedom which offers a high enough fidelity for most flight profiles, but if highly dynamic profiles were to be simulated a full six degree of freedom model could be investigated.

Since the simulator is designed to be used as a tool for studying the performance of any of the vast amount of hybrid configurations, the future uses are limitless. One of the ideas that is of considerable interest is to use the simulator for solving the optimization problem of minimizing fuel consumption. Since there are many ways to fly the aircraft and operate the hybrid propulsion system, an optimization problem could be set up to find a speed and altitude profile that minimizes fuel consumption, for example. Or, if using a parallel or series-parallel hybrid configuration, the torque split between the electric machine and thermal machine could be optimized for minimizing fuel consumption.

BIBLIOGRAPHY

[1] *Current Market Outlook 2016-2035.* Boeing, 2016.

[2] *Global Market Forecast: Mapping Demand 2016-2035.* Airbus, 2016.

[3] European Commission. *Flightpath 2050: Europe's Vision for Aviation.* Publications Office of the European Union, 2011.

[4] *IATA Resolution on the Implementation of the Aviation "CNG2020 Strategy".* International Air Transport Association, 2013.

[5] *Strategic Implementation Plan.* NASA Aeronautics Research Mission Directorate, 2019.

[6] Sandy Thomas. *Fuel Cell and Battery Electric Vehicles Compared.* H_2Gen Innovations, 2009.

[7] J.Y. Hung and L.F. Gonzalez. On parallel hybrid-electric propulsion system for unmanned aerial vehicles. *Progress in Aerospace Sciences*, 51:1–17, 2012.

[8] C. Friedrich and P.A. Robertson. Hybrid-electric propulsion for aircraft. *Journal of Aircraft*, 52(1):176–189, 1 2015.

[9] Tyler J. Wall and Richard T. Meyer. Hybrid electric aircraft switched model optimal control. *Journal of Propulsion and Power*, 36(4):488–497, 7 2020.

[10] Ye Xie, Al Savvarisal, Antonios Tsourdos, Dan Zhang, and Jason Gu. Review of hybrid electric powered aircraft, its conceptual design and energy management methodologies. *Chinese Journal of Aeronautics*, 34(4):432–450, 2021.

[11] Sergio Grammatico, Andrea Balluchi, and Ettore Cosoli. A series-parallel hybrid electric powertrain for industrial vehicles. In *2010 IEEE Vehicle Power and Propulsion Conference*, pages 1–6, 2010.

[12] K.T Chau and Y.S Wong. Overview of power management in hybrid electric vehicles. *Energy Conversion and Management*, 43(15):1953–1968, 2002.

[13] Tyler J. Wall and Richard Meyer. A survey of hybrid electric propulsion for aircraft. In *53rd AIAA/SAE/ASEE Joint Propulsion Conference*, 2017.

[14] Ralph D. Kimberlin. *Flight Testing of Fixed Wing Aircraft*. American Institute of Aeronautics and Astronautics, 2000.

[15] Jan Roskam. *Airplane Design Part I: Preliminary Sizing of Airplanes*. DARcorporation, 1997.

[16] Jan Roskam. *Airplane Design Part II: Preliminary Configuration Design and Integration of the Propulsion System*. DARcorporation, 1997.

[17] Snorri Gudmundsson. *General Aviation Aircraft Design: Applied Methods and Procedures*. Butterworth-Heinemann, first edition edition, 2014.

[18] Barnes Warnock McCormick. *Aerodynamics, Aeronautics, and Flight Mechanics*. Wiley, 2nd ed edition, 1995.

[19] Martin Hepperle. *Javaprop - Users Guide*. 2010.

[20] Robert A. McDonald. Modeling of electric motor driven propellers for conceptual aircraft design. In *53rd AIAA Aerospace Sciences Meeting*. American Institute of Aeronautics and Astronautics, 2015.

[21] *PowerPhase 125*. uqm. `https://wiki.neweagle.net/ProductDocumentation/EV_Software_and_Hardware/Traction_Inverters/UQM/PowerPhase_125_DataSheet.pdf`.

[22] *Manual for EMRAX Motors / Generators.* EMRAX, March 2020. https://emrax.com/wp-content/uploads/2020/03/manual_for_emrax_motors_version_5.4.pdf.

[23] Javier Gazzarri, Robyn Jackey, Tarun Huria, and Massimo Ceraolo. High fidelity electrical model with thermal dependence for characterization and simulation of high power lithium battery cells. IEEE, 2012.

[24] *Battery (Table-Based).* Mathworks. https://www.mathworks.com/help/physmod/sps/ref/batterytablebased.html.

[25] Tingshu Hu, Brian Zanchi, and Jianping Zhao. Simple analytical method for determining parameters of discharging batteries. *IEEE Transactions on Energy Conversion*, 26(3):787–798, 2011.

[26] *31Ah Lithium-ion Datasheet.* Kokam.

APPENDICES

Appendix A

LYCOMING O360-A PERFORMANCE CHART

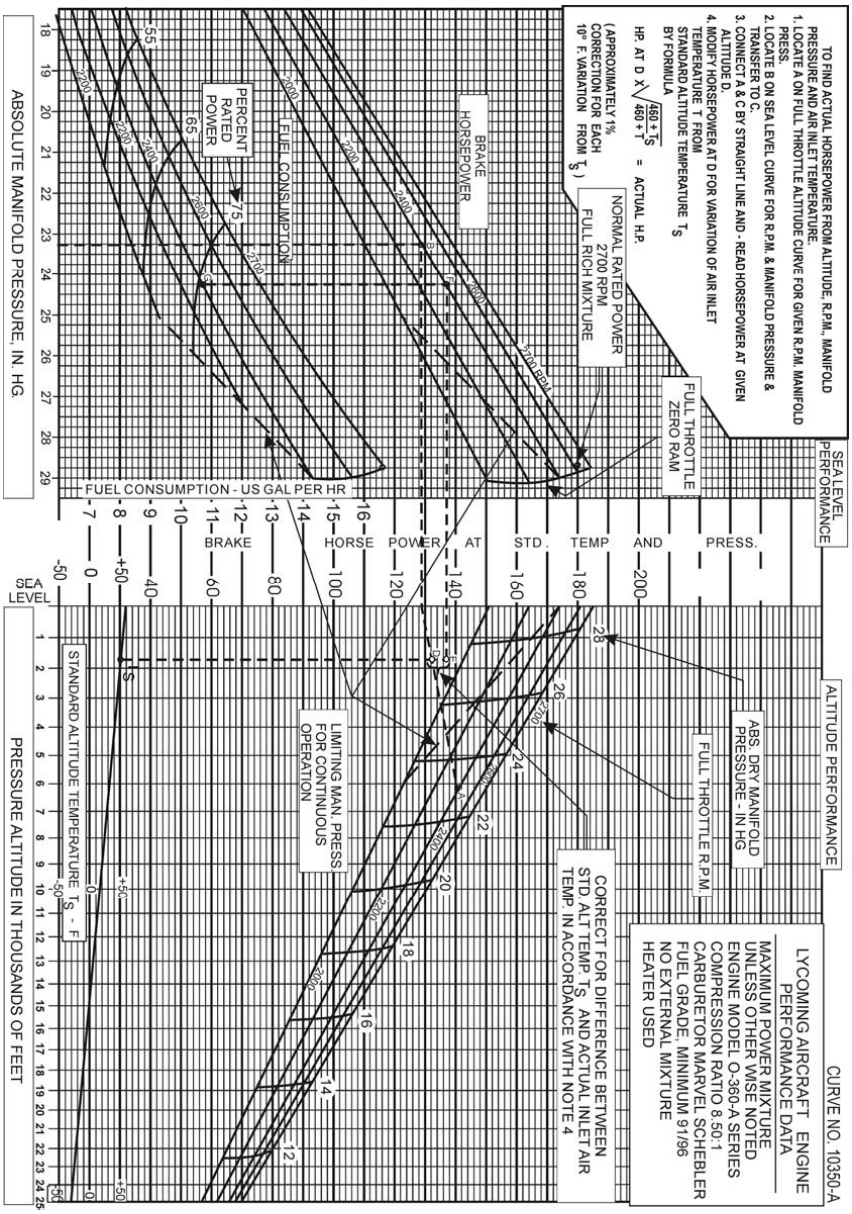

Figure A.1: Lycoming O360-A Performance Chart